Bioactive Materials 6 (2021) 2089–2104

Contents lists available at ScienceDirect

Bioactive Materials

journal homepage: www.sciencedirect.com/journal/bioactive-materials

Cellulose fibers-reinforced self-expanding porous composite with multiple hemostatic efficacy and shape adaptability for uncontrollable massive hemorrhage treatment

Yansen Wang [a], Yifan Zhao [b], Longxue Qiao [c], Faxing Zou [a], Yajie Xie [a], Yudong Zheng [a,*], Yong Chao [c,**], Ying Yang [d], Wei He [a], Siming Yang [e,***]

[a] School of Materials Science and Engineering, University of Science and Technology Beijing, Beijing, 100083, PR China
[b] Department of Anesthesiology, Medical College of Chinese PLA, Beijing, 100853, PR China
[c] Department of Medical Engineering, The First Affiliated Hospital of the PLA General Hospital, Beijing, 100048, PR China
[d] First Affiliated Hospital of Medical College, Zhejiang University, Hangzhou, 310003, PR China
[e] Key Laboratory of Wound Repair and Regeneration of PLA, Chinese PLA General Hospital, Medical College of PLA, Beijing, 100853, PR China

ARTICLE INFO

Keywords:
Porous materials
Cellulose fibers
Self-expanding ability
Shape-adaptive
Hemostasis

ABSTRACT

Uncontrollable hemorrhage leads to high mortality and thus effective bleeding control becomes increasingly important in the military field and civilian trauma arena. However, current hemostats not only present limitation when treating major bleeding, but also have various side effects. Here we report a self-expanding porous composites (CMCP) based on novel carboxymethyl cellulose (CMC) fibers and acetalized polyvinyl alcohol (PVA) for lethal hemorrhage control. The CMC fibers with uniform fibrous structure, high liquid absorption and procoagulant ability, are evenly interspersed inside the composite matrix. The obtained composites possess unique fiber-porous network, excellent absorption capacity, fast liquid-triggered self-expanding ability and robust fatigue resistance, and their physicochemical performance can be fine-tuned through varying the CMC content. *In vitro* tests show that the porous composite exhibits strong blood clotting ability, high adhesion to blood cells and protein, and the ability to activate platelet and the coagulation system. *In vivo* hemostatic evaluation further confirms that the CMCP presents high hemostatic efficacy and multiple hemostatic effects in swine femoral artery major hemorrhage model. Additionally, the CMCP will not fall off from the injury site, and is also easy to surgically remove from the wound cavity after the hemostasis. Importantly, results of CT tomography and 3D reconstruction indicate that CMCP can achieve shape adaptation to the surrounding tissues and the wound cavities with different depths and shapes, to accelerate hemostasis while protecting wound tissue and preventing infection.

1. Introduction

Uncontrollable bleeding is a major global problem, which can lead to significant mortalities in military or civilian populations [1,2]. A huge number of deaths occur each year because of ineffective bleeding control [3,4]. For patients with sudden and unexpected major bleeding, uncontrollable large vessel bleeding and extensive bleeding from trauma tissue are the reasons to high rates of death [5,6]. Prompt and effective prehospital/first-aid hemostatic technologies and hemostats can gain invaluable time for subsequent therapy and therefore reduce the disability and mortality.

Currently, there are several first-line first-aid hemostatic materials equipped by the military, such as HemCon (HemCon Medical Technologies, Oregon, USA) [7], Celox (MedTrade Products Ltd, UK) [8], WoundStat (TraumaCare Inc., USA) [9] and Quikclot (Z-Medica Inc., USA) [10]. However, these hemostats have been proved only effective for mild to moderate bleeding, and their hemostatic effect is not strong enough to deal with large and uncontrollable blood vessel bleeding.

Peer review under responsibility of KeAi Communications Co., Ltd.
* Corresponding author.
** Corresponding author.
*** Corresponding author.
E-mail addresses: zhengyudong@mater.ustb.edu.cn (Y. Zheng), yongchg@263.net (Y. Chao), ysm0117@126.com (S. Yang).

https://doi.org/10.1016/j.bioactmat.2020.12.014
Received 24 July 2020; Received in revised form 30 November 2020; Accepted 17 December 2020

Additionally, issues caused by using these hemostats during the hemostasis progress including large side effects, high re-bleeding rates (HemCon&Celox) [7], embolic risks (WoundStat), tissue damage and debilitation (Quikclot) [11,12], also seriously limit their further applications. Besides, other hemostatic materials containing animal-derived ingredients such as collagen, fibrinogen or thrombin may produce allergic reactions or immunogenicity, and cause nerve damage or compression of body due to their excessive swelling when used *in vivo*. Generally, to achieve rapid clinical hemostasis, ideal hemostatic materials need to meet the following requirements: a) strong liquid absorption capacity; b) suitable mechanical properties to withstand blood pressure, compression and friction with surrounding tissues; c) maintain structural stability in extreme conditions and cause no damage to wound tissue; d) good biocompatibility; e) easy and fast operation. However, none of the currently used hemostats can meet all these requirements, thus more researches are required to develop novel bio-safe and more efficient hemostats for hemorrhage control and the treatment of specific wounds.

Various naturally derived materials has gradually become independent or integrated components of many hemostatic materials, as they showed the abilities to stimulate coagulation system while reducing immunogenicity risks. Products made of cellulose fibers such as cotton pads, gauze and foam have been already widely used as simple surgical hemostatic equipment in military or civilian field because cellulose are abundant in nature and easy to manufacture [13,14]. The results of actual application indicated that, when directly applied on a bleeding wound, these products may only provide partial hemostatic reaction via limited absorbing blood, and additionally, they can easily adhere to wound tissue which can be a potential problem during their subsequent removal. Therefore, the focus of studies has gradually shifted to use chemical modification to improve the hemostatic efficiency of the cellulose fibers while reducing their risks during removal. Modified cellulose refers to the control of cellulose fiber structure in which the primary and secondary alcohol moieties are oxidized and converted to carboxyl or aldehyde groups, which can prominently regulate its physicochemical properties [15,16]. Except the contact activation of the blood coagulation cascade, the acidic pH and the negative charges of these modified cellulose fibers are also considered to induce platelet aggregation, activation, and stimulate intrinsic pathway of the coagulation system. Modified cellulose-based materials are also reported to be biodegradable via enzymatic (glycosidase-based) and macrophagic processes [17], and the low pH generated by their chemical groups can inhibit the growth of some bacterial strains [18]. Recent studies have found that modified cellulose can be uniformly dispersed in the matrix of synthetic polymers (PVA, PAA, etc.) or natural polymers (fibrin, chitosan, alginate, etc.) to not only enhance their mechanical properties but also impart clotting properties to the polymer materials [19,20].

Large number of porous materials that have been extensively developed show great potential in stopping major bleeding due to their favorable properties, such as high surface area and porosity, ability to rapidly absorb liquid [21,22], and good compatibility with common hemostatic agents [23,24]. Among them, self-expanding porous materials which simultaneously possess absorption capacity, sealing and tamponade effect are gradually used as scaffolds or matrix materials to develop hemostatic materials or technologies. One of the expanding porous material used for rapid hemostasis in military field has already been cleared and approved by FDA and named XSTAT (RevMedx, Wilsonville, USA). XSTAT consists of cellulose sponges coated with chitosan [25]. After absorbing blood, the sponges can axially expand several times its original volume within a very short period of time. XSTAT has been experimentally proved to be effective to achieve hemostasis in multiple severe hemorrhaging animal models (groins, arteries, and livers, ect) [26]. However, due to that XSTAT is composed of miniature cellulose sponges with limited volume expansion and mechanical strength, a large amount of sponges (more than 90) are needed to fill the wound cavity when applied to the hemorrhaging site, and the required hemostatic time as well as the time and difficulty to remove all sponges postoperation will inevitably increase correspondingly. Self-expanding porous materials made of synthetic polymers have also been reported possessing excellent hemostatic capability in treating heavy bleeding wounds. One recently reported self-expanding porous materials composed of shape memory polyurethane (SMP) foams possessed high volume expansion rate and water uptake ability which would allow for easy delivery into narrow, penetrating wounds, and subsequent expansion to completely fill abnormal wound boundaries with a single device [27,28]. Besides, researches also show that self-expanding porous hydrogels with rapid blood-triggered self-expanding ability show excellent hemostatic capability in treating lethal noncompressible hemorrhage [29]. Our previous research also found that the self-expanding foam composed of polyvinyl alcohol (PVA) and alginate exhibited hemostatic effects on treating femoral artery bleeding caused by firearm [30].

The aim of this study was to improve current materials and technologies used for hemorrhage control and irregular wound treatment by developing novel hemostats with large volume-filling capabilities and rapid clotting abilities. Acetalized PVA with porous structure, which is prepared by chemically crosslinked PVA with aldehyde (formaldehyde, glutaraldehyde, etc.) [31,32], not only inherits the deformability and flexibility of porous materials but also exhibits excellent liquid absorption capacity and high liquid-triggered expansion [33]. Cellulose fibers are widely used to enhance the mechanical properties of materials and carboxymethyl modification can endow them with hemostatic ability. Therefore, introducing CMC into acetalized PVA will be greatly effective for reinforced mechanical strength and hemostasis. In this study, a series of hemostatic self-expanding porous composites composed of acetalized PVA and novel biocompatible CMC were successfully developed. The microstructure, liquid absorption, mechanical performance and hemostatic capacity of the novel CMC fibers were first studied. Then, the CMC fibers with high liquid absorption and good hemostatic capacity were evenly interspersed inside the composites. The effect of CMC content on the physicochemical properties and biocompatibility of the composites were systematically investigated. Subsequently, *in vitro* hemostatic performance of the composite including adhesion and activation of blood cells, and the abilities to promote thrombus formation and activate coagulation pathways were successively evaluated. Further, the composites were used to treat swine femoral artery lethal injury, and hemostatic time and blood loss were measured to investigate the hemostatic efficacy of the composites. Finally, Micro-CT and 3D reconstruction were used to study the shape-adaptive ability of composites to wound cavity and tissues.

2. Material and methods

2.1. Materials

TENCEL™ fibers were purchased from Lenzing (Austria). PVA particles (polymerization degree of 1700 and alcoholysis degree of 99%) and calcium chloride were purchased from China Sinopharm Group Co., Ltd. LDH (lactate dehydrogenase) was purchased from Shanghai Aladdin Reagent Co., Ltd. APTT and PT assay reagents were received from Sigma-Aldrich Co. Ltd. L929 cells was provided by Institute of Orthopedics, Chinese PLA General Hospital, Beijing. Fluo-4 AM was purchased from Beijing Solarbio Science & Technology Co., Ltd. Cell Counting Kit-8 (CCK-8), LG-DMEM and Calcein AM·PI were purchased from Dojindo (Japan), Shanghai yuanye biotechnology Co., Ltd and Shanghai yaji biotechnology Co., Ltd, respectively. Deionized water was offered by University of Science and Technology Beijing. All other reagents were analytical grade and used as received.

2.2. Preparation of CMC and CMCP composites

TENCEL fiber is a new generation of biocompatible green fiber with excellent flexibility and toughness, and its wet strength is much better

than common cotton fibers. In this work, TENCEL fiber was used as the original cellulose fiber. Sodium hydroxide was dissolved in 50% ethyl alcohol solution to prepare a sodium hydroxide solution with a mass fraction of 8%. TENCEL fibers were immersed into the solution at room temperature for 1 h. Then, 10% sodium chloroacetate solution was added, and the mixture was gently stirred in an oil bath at 35 °C for 30 min. Then the temperature was raised and the mixture was stirred at 75 °C for 30 min, 60 min and 90 min, respectively. After the mixture cooled down, the fibers were taken out and washed several times with a 75% ethanol solution containing acetic acid until neutral. Finally, the fibers were dehydrated with absolute ethyl alcohol and dried at 40 °C for 2 h to obtain the carboxymethylated cellulose fibers. According to reaction time, from 30 min to 90 min, the fibers were named CMC1, CMC2, and CMC3 in order.

Calcium chloride solution with concentration of 0.1 mol/L was dropwise added on the surface of CMC until CMC reached a fully swelling state. The CMC and Ca^{2+} mixture with different mass fractions were added into a 10% PVA aqueous solution to prepare a gel-like mixture. The mixture was stirred and left standing for 30 min to obtain even distribution of the components. Aldehyde (molar ratio of PVA/aldehyde was 1) solution and a small amount of acid were subsequently added to the mixture at room temperature until well mixed. Then, the mixture was foamed through supercritical fluid technology, with supercritical CO_2 as the foaming agent. Finally, the foamed mixture was directly placed into molds and underwent vacuum freeze drying. The as-prepared porous composite with different CMC content (5, 10 and 15 wt%) were named as CMCP-1, CMCP-2 and CMCP-3, respectively.

2.3. Structural characterization

FT-IR spectra of different materials were obtained on a TENSOR II spectrometer (Bruker, Germany). The spectra were taken over the wavenumber range of 600–4000 cm^{-1}, with a scanning resolution of 4 cm^{-1}, and each sample was scanned for 15 times. The morphology of the samples was observed using a SU8020 (Japan) field emission scanning electron microscope (FE-SEM) operating at 10 kV. Samples were freeze-dried and sputtered with gold before observation. The average pore sizes were determined from the optical microscopy (OM) (BK300. OPTEC, China) images of different materials using Image J software (Version 1.50 h. National Institutes of Health, U.S.). The porosity of different materials was measured by mercury intrusion method through using a PoreMaster 33 mercury porosity analyzer.

2.4. Expansion properties

The volume expansion (V_E) of CMCP composites was analyzed using the following Eq (1).

$$V_E = \frac{V_n}{V_0} \times 100\% \quad (1)$$

where V_0 and V_n refer to the volume of samples before and after self-expansion, respectively.

The dynamic expansion force test of materials was performed based on the method described in previous literature [27,30]. Cylindrical sample (50 mg) with a diameter of 9 mm and a height of 5 mm was used in this test. Briefly, the sample was placed between the compression platen and the operate board of the Texture Analyzer (TAXT plus, Stable Micro Systems, UK). Trigger force of 0.1 N was applied before the test started. After pre-loading, citrated whole blood (collected from healthy donors) was added to initiate the expansion of sample. The distance between the compression platen and the operate board remained constant throughout the test, while the expansion force exerted by the expansion of the sample was continuously measured for 5 min. The buoyancy force exerted by blood was also measured. The dynamic expansion forces were calculated through subtracting the buoyancy force from the raw force.

2.5. Anti-impact test

The anti-impact experiment was performed according to the methods described in previous studies [34]. Briefly, a circular cavity with diameter of 2.5 cm were created in the center of a fresh porcine thigh tissue, and a syringe pump filled with phosphate buffered saline (PBS, 0.05 mol/L, pH = 7.4 ± 0.2) was connected to the bottom of the tissue cavity. After the experiment started, the syringe pump started to pump PBS into the cavity. As soon as PBS flowed out of the hole on the top of the tissue cavity, the materials (particles with diameter of 9 mm and height of 5 mm) were filled into the tissue cavity immediately. A data acquisition system was used to measure the generated stress. The flow rate of the solution was constantly increased via the pump to exert a continuous and increasing pressure on the materials in the cavity. The stress required to push the samples out of the tissues were recorded to simulate the stress of the arterial blood flow impacting the samples in the wound cavity. The maximum stress before pressure loss was considered the anti-impact force. Medical gauze was tested under the same conditions. All the tests were repeated three times.

To visually observe the expansion performance of the CMCP, and its shape adaptability to the tissue, a random shaped cavity (30-mm wide, 40-mm high, and 100-mm long) was created in a piece of porcine thigh muscle tissue. The contrast agent combined samples were then crammed into the cavity followed by adding fresh whole blood. After sufficient interactions, the position of the CMCP samples in tissue as well as their shape changes during absorbing blood were observed using Micro-CT.

2.6. Water absorption capacity

Samples were cut into the same form and the dry weight (W_0) of each sample was measured before the test. Then, the dry samples were immersed in deionized water at 37 °C and incubated for 10 min to make them reach the saturated water absorption. At different time points, the samples were then taken out and gently dabbed on filter papers to remove the excess water on the surface, and the wet weight of the samples (W_t) was immediately measured. The water absorption capacity (Q) was calculated as Eq (2):

$$Q = \frac{W_t - W_0}{W_0} \times 100\% \quad (2)$$

2.7. Mechanical properties

Tensile and compress testing was conducted on a TA-XT plus texture analyzer with a constant speed of 2 mm min^{-1}. The size and shape of the samples accorded with ASTM D 638–2003 Type IV specimens. For each sample, triplicate tests were carried out.

2.8. Cell culture

L929 cells were cultured in DMEM containing 10% fetal bovine serum (FBS, Gibco, Thermo Fisher Scientific, USA) and 1% penicillin-streptomycin (FBS, Gibco, Thermo Fisher Scientific, USA). The cells were maintained on humidified incubator (Panasonic MCO-18AC, Japan) with 5% CO_2 at 37 °C.

CCK-8 assay: Samples were placed in a 48-well plate and sterilized by ultraviolet irradiation for 60 min. L929 cells were then seeded on the sample surface at a density of 5×10^4 cells cm^{-2}. After culturing for 1, 3 and 7 days, respectively, samples were taken out and placed in culture dishes, and 100 μL of serum-free DMEM medium and 10 μL of CCK-8 reagent were added to the culture dishes. After incubation at 37 °C for 4 h, the absorbance of the supernatant was measured at 450 nm on a microplate reader (MULTISKAN MK3, Thermo, USA).

Live/Dead staining: Samples were put in a 48-well plate, and a suspension of L929 cells in the fibroblast medium was added to each well at a density of 5×10^4 cells cm^{-2}. The plate was incubated at 37 °C in 5% CO_2. On day 1, 3 and 7 after incubation, the fibroblast medium was replaced by PBS solution containing 1.5 μL propidium iodide and 1 μL calcein-AM (Calcein-AM/PI Double Staining Kit, Japan) and incubated for another 30 min. Then the samples were gently washed with PBS and then observed under a fluorescence microscope.

2.9. Adhesion and activation of blood cells

Fluorescence intensity (FI) of Ca^{2+}: 10 mL of human blood was collected in an anticoagulation tube (Sodium citrate). The blood was centrifuged at 200 r min^{-1} for 15 min to obtain platelet-rich plasma (PRP). 500 μL of PRP was added to centrifuge tube (1.5 mL), centrifuged at 1500 r min^{-1} for 15 min, and the supernatant was removed. Then, 10 μL of Fluo-4 AM was mixed with the platelets and incubated for 15 min at 37 °C in dark conditions. Subsequently, sample (10 mg) was added to the tube and incubated at 37 °C for 15 min, and then 200 μL of 1% Triton-100 was added. The mixtures were centrifuged at 12,000 rpm, and 100 μL of supernatant in each tube was transferred to one of the holes in a 96-well plate. FI was measured using a Spectral Scanning Multimode Reader (Thermo Scientific Varioskan Flash, USA) at an excitation of 494 nm and emission of 516 nm. The effect of Ca^{2+} in the material had been taken into account when calculating the FI and the percentage of intracellular Ca^{2+}. The control group (PRP only) was tested using the same method as above. Each group was measured in triplicates.

The sample was first immersed in the PRP and incubated at 37 °C for 30 min. Then, the sample was rinsed with PBS solution for three times and incubated in PBS with 1% Triton X-100 at 37 °C for 1 h. Subsequently, the sample was incubated in 2.5% glutaraldehyde, dehydrated using a gradient ethanol solution (30, 50, 70, 90 and 100%) and went through freeze-drying. The morphology of platelets on the sample after incubation were observed through FE-SEM (FV1000, Olympus, Japan). The number of platelets on the samples was also quantified using a Lactate dehydrogenase (LDH) assay kit (Sigma, Aldrich) by measuring the LDH released from the lysed platelets [35].

Concentration of CD61 and CD62P (P-selection): The whole blood was centrifuged at 200 r min^{-1} for 15 min, and 100 μL of the upper PRP was taken in each EP tube. Then, sample (10 mg) was added and incubated at 37 °C for 30 min. Next, 1 mL PBS was added to each tube, and the sample was rinsed and taken out from the tube. The remaining mixture was centrifuged at 1500 r min^{-1} for 15 min, and the supernatant was removed. 50 μL of FITC (Shanghai Macklin Biochemical Co., Ltd) labeled anti-CD61 and anti-CD62p (Sino Biological, China) were added after dilution, and the mixture was kept in the dark at 4 °C for 20 min. The concentration CD61 and CD62p was detected using BD Accuri C6 flow cytometer.

2.10. Hemostasis in vivo

In vivo experiments were strictly performed accorded with the Guide of National Research Council for the care and use of laboratory animals. The final criteria for hemostasis were no obvious bleeding, no active bleeding and no exudate at the wound site. Prior to testing, all the samples were sterilized by cobalt-60 radiation (15 K) for 1 h.

Liver injury model: Sprague-Dawley (SD) rat (male, 250 g, 5–6 weeks old, n = 18) were provided by Chinese PLA General Hospital. The rats were restrained and anesthetized with 1.5% isoflurane. Eighteen rats were randomly grouped into control, Gauze, and CMC2 groups (n = 6 for each group). The middle lobe of the liver of SD rats was cut to expose. Incision (2 cm) on the liver was created using a scalpel to initiate bleeding [35]. Serous fluid around the liver was carefully removed to prevent inaccuracies in the estimation of the blood weight obtained by the filter papers. CMC sample (3 × 3 cm) was immediately put on the liver cut, and started to record the time. The spilled blood was sucked by a piece of pre-weighed filter paper every 10 s until the hemostasis process was complete. Then the weight of the sample as well as the filter paper with absorbed blood was measured to calculate the mass of total blood loss. In the other experimental group, the cut was treated standard medical gauze until the bleeding stopped. Group without any treatment was used as a blank control.

Femoral artery injury model: The femoral artery injury experiment was performed based on the method described in previous studies [36,37]. Bama miniature pigs (n = 12, female, weighing 24.5 ± 2.1 kg) were used in the experiment. Before operation, the pigs were restrained, pre-anesthetized by injecting 10 w% chloral hydrate (0.5 mL/100 g). The pigs were then fixed in the supine position on the 37 °C thermostatic operation table. One side of the carotid artery was separated, intubated, and connected to MP150 multi-channel physiological monitor to dynamically monitor the heart rate and base mean arterial pressure (MAP) of the pigs before surgery. The surgical procedures were performed by standard aseptic methods. The ear vein of each pig was cannulated, and Lactated Ringer's (LR) solution (5 mL/kg) was administered to compensate for fluid loss. The left femoral artery was cannulated for monitoring and recording of blood pressure, heart rate, electrocardiogram, and body temperature of the animals during the whole experiment. In order to obtain more accurate experimental data, the carotid artery was also monitored, and the recorded data were used as standby data. The pigs were randomly divided into control group (n = 4), Combat gauze group (n = 4) and CMCP group (n = 4). To create a severe hemorrhage in the groin area, approximately 4–5 cm of the right femoral artery was dissected and freed from the surrounding tissues, and then the overlying muscle was removed. The artery was then treated with 10 mL of 5% lidocaine to prevent vascular contraction and vascular spasm. A stabilization period (10 min) was allowed, and then baseline data, including the MAP and other vital signs, were recorded. A stable MAP of 60 mmHg or higher was required before the experiment. The artery was first clamped proximally and distally, and then severed using a surgical scissor. The clamps were immediately released, and free bleeding was allowed for 30 s. The flowing blood was collected with gauze, weighed and recorded as the pretreatment blood loss. While the femoral artery was bleeding, CMCP samples were immediately injected into the wound cavity using a self-made injector with diameter of about 3 cm, and manually compressed against the wound with slight pressure to keep the composites inside the wound. The compression was performed by the same operator in the same way for each animal. Combat Gauze was packed in the bleeding wound in the other group. The injury site was visually checked every 30 s, and the time was recorded when the hemostasis process was complete. The volume of postoperative blood loss was calculated from the change in the weight of gauze and the samples (Combat gauze or CMCPs). The total blood loss was expressed as the sum of the pretreatment blood loss and the posttreatment blood loss. If hemostasis was not achieved or if re-bleeding occurred within 3 min, the sample was removed and replaced with another one. If hemostasis was achieved and was stable for 10 min, the animal was resuscitated intravenously to its baseline MAP with LR solution. Animal survival was defined as the presence of heart beats at the end of 180 min.

2.11. Statistical analysis

The experimental data were analyzed by one-way analysis of variance (ANOVA) using SPSS6.0 (Statistical Product and Service Solutions). The data were presented as means ± standard deviation (SD). p value < 0.05 was considered statistically significant.

3. Results and discussion

3.1. Characterization of the CMC fibers

The strategy for fabricating CMC fibers is illustrated in Fig. 1a. The FT-IR curves of all the CMC samples contained three characteristic

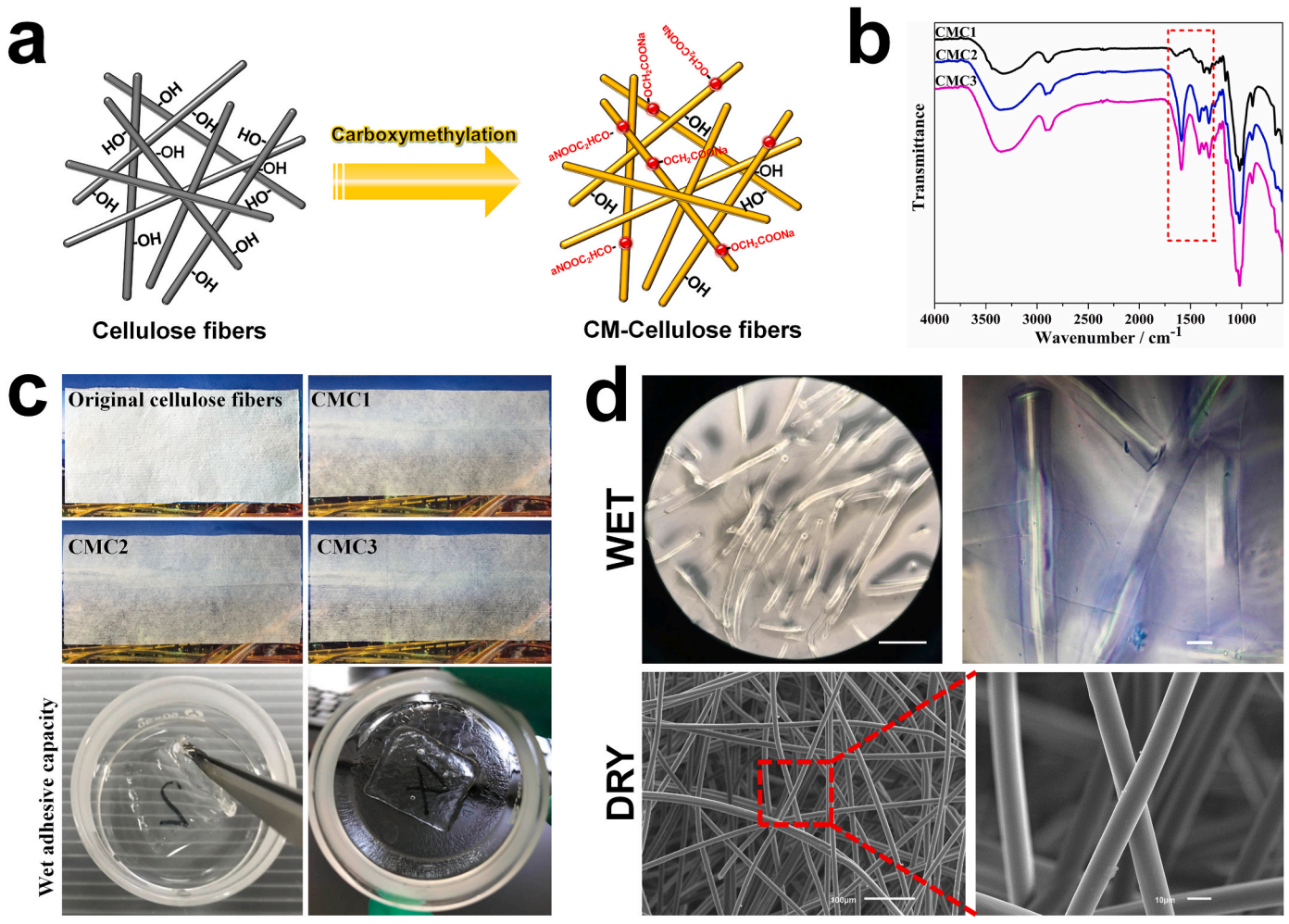

Fig. 1. a. Schematic diagram of the fabrication of CMC fibers. **b**. FTIR spectra of different CMC samples. **c**. Macroscopic observation of different cellulose samples (5 cm × 12 cm) and the CMC samples (2 cm × 2 cm) in wet state. **d**. The microstructure of the CMC in dry and wet state.

absorption peaks of cellulose at 3300, 2850, and 1050 cm^{-1}, which were assigned to the stretching vibrations of the n(-OH), n(-CH_2), and n(C–O) groups, respectively. By contrast, new absorption peaks appeared at 1560 and 1420 cm^{-1} were assigned to the C═O stretching vibrations of the carboxymethyl groups, indicating the successful grafting of carboxymethyl groups on the cellulose molecular chains. In addition, the intensity of these new absorption peaks varied with the degree of carboxymethyl substitution (Fig. 1b). Compared with the original cellulose fibers, the transparency of the carboxymethyl modified samples was greatly improved in the dry state. After carboxymethyl modification, the cellulose fibers showed the ability to rapidly absorb water, and became almost transparent after complete water absorption. In addition, the CMC fibers would not collapse and exhibited certain mechanical strength and adhesive capacity (adhere to the glassware) in the wet state (Fig. 1c). The microstructure of the CMC could be observed in Fig. 1d. CMC showed typical fibrous network structure in its dry state, long fibers with a diameter less than 10 μm, were intertwined together. After absorbing water, a part of long fibers broke into shorter ones with the same diameter, and the entangled fibers also became dispersed. CMC fibers showed certain water holding capacity owing to their carboxyl groups, and they would swell while rapidly absorbing water. Therefore, the diameter of the CMC fibers in wet state became slightly larger than that of the original fibers.

CMC fiber bundles maintained good strength and flexibility in the dry state. When putting one end of the fibers into water, the water could be rapidly absorbed from the bottom up. After completely absorbing water, the fibers became almost transparent and showed a certain strength, and the absorbed water would not seep under pressure (Fig. 2a). The modified fibers also exhibited excellent spinnability and could be spun into uniform fibrous cloths with high deformability (Fig. 2b).

As a vital criteria to evaluate the efficiency of carboxymethylation, degree of substitution (DS) of CMC was determined using the acid-base titration method [38,39]. As is shown in Fig. 2d, CMC with different degree of substitution were prepared by controlling the reaction time, and the DS gradually increased from 0.34 (CMC1) to 0.68 (CMC3) with carboxymethylation time increasing from 30 min to 90 min. With the increase of the DS, the volume swelling ratio and the liquid adsorption capacity of carboxymethyl cellulose fibers gradually increased (Fig. 2c and e). It is worth noting that the CMC fibers with high degree of substitution did not dissolve in water and still maintained the original fibers structure after swelling. Before carboxymethyl modification, strong binding force (hydrogen bonds) formed through the interaction of hydroxyl groups existed among cellulose fibers. However, after carboxymethylation, some carboxymethyl groups substituted the hydroxyl groups, leading to the decrease of the amount of hydroxyl groups on microfibers. Therefore, the increase of DS reduced the bonding force among cellulose fibers, resulting in a significant decrease in mechanical strength and toughness of the CMCs (Fig. 2f). Besides, the repulsive force between carboxymethyl groups would also reduce the bonding force between the fibers, thereby resulting to the decrease of the mechanical strength of CMCs. Fibers with DS of 0.47 (CMC2) possessed large

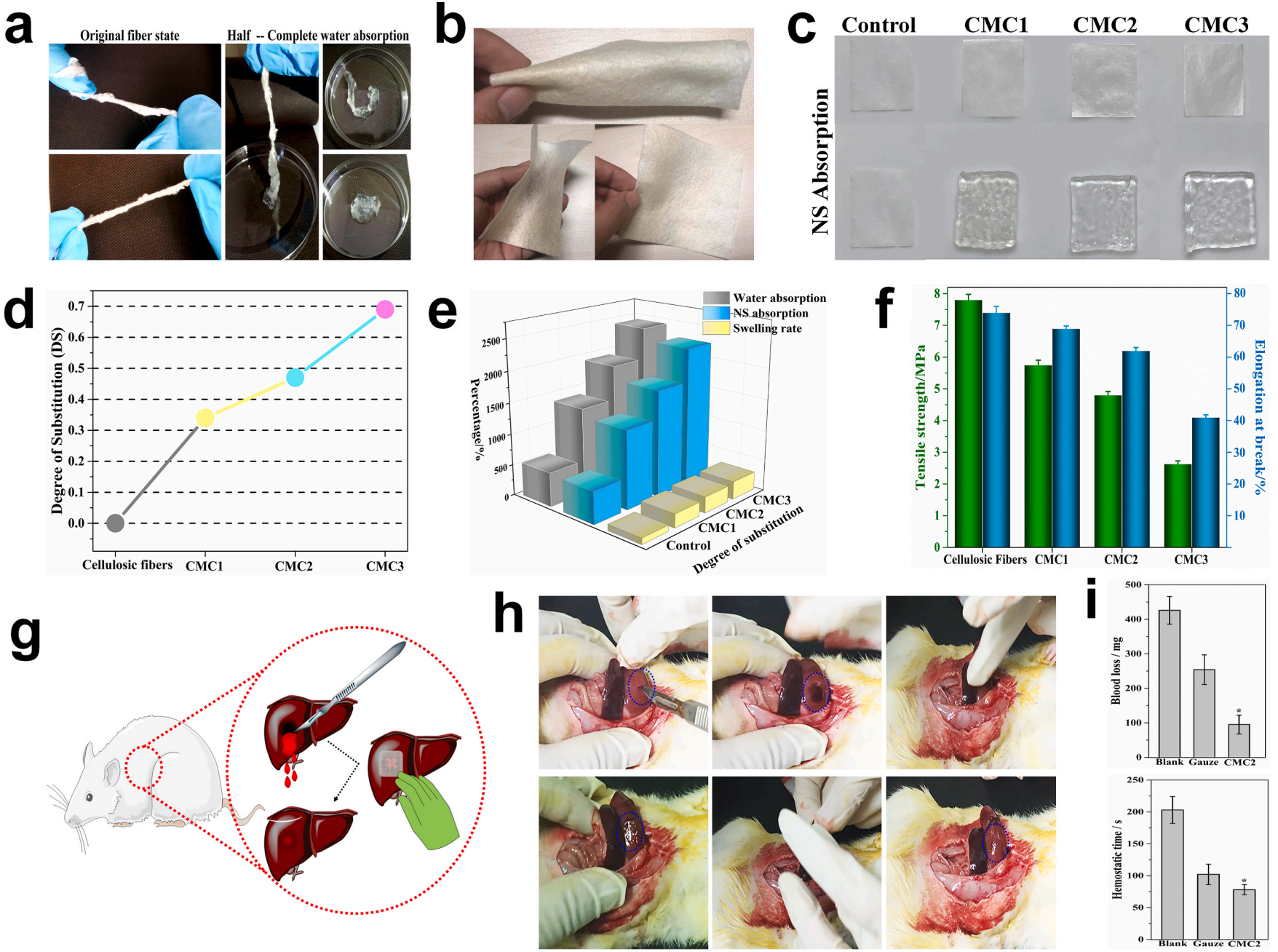

Fig. 2. **a**. The original morphology of the CMC and the change of the morphology during water absorption. **b**. The CMC fibers can be spun into fiber cloth (10 cm × 10 cm) with excellent flexibility. **c**. Macroscopic images of cellulose fibers (2 cm × 2 cm) and different CMC fibers before and after absorbing normal saline. **d**. The relationship between the DS of different CMC samples and the reaction time. The swelling ratio, adsorption capacity (**e**) and the mechanical strength and toughness (**f**) of CMC with different DS. Schematic representation (**g**) and macroscopic images (**h**) of the *in vivo* hemostatic evaluation of the CMC2 using rat liver hemorrhage model. **i**. Blood loss and hemostatic time. Error bars, mean ± s.d. *p < 0.05, represents significant difference compared with blank group. This *in vivo* hemostasis experiment has been successfully repeated in rats >10 times, demonstrating the reliability of the CMC treatment.

number of carboxymethyl groups while maintaining the flexibility and mechanical strength of cellulose fibers, and therefore, it was chosen for the subsequent experiments.

To evaluate the hemostatic performance of CMC2, a rat liver injury model was established (Fig. 2g) [40]. Medical gauze was employed as control. After 5 s of free bleeding, the bleeding site was treated with CMC2. During the hemostasis process, blood around the wound was rapidly absorbed by CMC2, and then CMC2 swelled and formed gel-like "blood clots" as physical barriers to prevent blood from flowing out. After achieving complete hemostatsis, the CMC2 could be easily removed, and the wound site did not re-bleed (Fig. 2h). Among all the groups, CMC2 group showed the lowest blood loss of 92.7 ± 25.1 mg (n = 6). The blood loss of the blank group and gauze group was 429.3 ± 42.2 mg (n = 6) and 253.5 ± 47.9 mg (n = 6), respectively, which was significantly much higher than that of CMC2 group (Fig. 2i). Note that the CMC with high water absorption capacity would inevitably absorb small amounts of body fluids, resulting to that the obtained value of blood loss was slightly larger than actual blood loss. Additionally, the hemostatic time of the CMC2 group was significantly shortened compared with that of the gauze group and the blank group. All the rats in the CMC2 group were alive during and after the experiments.

3.2. Microstructure and morphology of the composites

The fabrication of the CMCP composites was schematically represented in Fig. 3. SEM images of both PVA porous material and CMCPs exhibited interconnected 3D porous structures. Compared with PVA, CMCPs had flatter surfaces as well as uniform and compact macrostructure. Moreover, large numbers of CMC fibers could be observed inside the CMCP, which both located in the interior pores and interspersed inside the composite matrix (Fig. 3b). PVA showed a large number of pores on its surface with average pore size over 200 μm. After incorporating with CMC, the porosity, pore size and total pore area of the CMCP composites decreased with the increasing CMC content, whereas the pore size distribution gradually became uniform (Fig. 3c). The uniformly distributed CMC increased specific surface area and the number of bonding sites inside the composites, and enhanced the intermolecular force between PVA and CMC, endowing the composites with a uniform and dense network structure.

The schematic representation of CMCP absorbing water and undergoing self-expansion was presented in Fig. 3d. CMCP would instantly self-expand when contacting water, one of the reasons is that water entered the interior of the composite through hydrophilic interaction and capillary action, induced the swelling of CMC while gradually filled all the pores in the interior, and subsequently initiated the volumetric expansion. Another possible reason is that water entered the interior of the composite, interacted with acetalized PVA molecules in the matrix through hydration, and then immobilized by PVA molecules, leading to the increase of gaps between the molecular chains (schematic diagram of this mechanism is shown in Fig. S1). In addition, due to that CMCP possessed high porosity and low relative density, after compression, the probability of entanglement or aggregation of the molecular chains was greatly reduced, and therefore the composite showed strong ability to recover to its original state after the external force was removed. After dehydration and fixing, the water filled in the internal pores was squeezed out, the binding effect between water and PVA disappeared, and the intermolecular entanglement was significantly enhanced, leading to a shape fixed state of the composite.

The morphology of the CMCP composite before and after absorbing water corresponded with the self-expanding mechanism and was also shown in Fig. 3d. The surface of CMCP in its original state and dry state showed the collapse of inner pores and networks caused by efflux of water and entanglement of molecular chains. While after absorbing water, the surface of the CMCP exhibited well-defined 3D porous network structure with uniform interconnected pores on it.

3.3. Cytocompatibility of the composites

L929 cells incubated in the extract of materials after culturing for 1, 4 and 7 days were used to evaluate the cytotoxicity of different materials. For all the tested samples, the number of cells increased continuously during the 7 days of culture, demonstrating their favorable cytocompatibility. CMCP composites exhibited better cell biocompatibility with cell number higher than that of the control group on each counting day (Fig. 4a). The biocompatibility of the materials and material-cell interactions were further evaluated and observed by cell adhesion experiment. After 7 days of incubation, cells had completely spread to the entire the surface and grown along the pores into the interior of the CMCPs (Fig. 4b). CMCP-3 with higher CMC content showed better ability to facilitate cell proliferation than CMCP-2, which may be due to the increased contact sites between cells and materials due to higher CMC content in CMCP-3. In general, scaffold architecture affects cell binding and spreading [41]. When cultured on macroporous materials (PVA porous material) or flat surfaces (cellulose fibers), cells have fewer binding sites on materials, and cell phenotype and growth tend to be flat and spread, which reduces the cell proliferation rate. While scaffolds combining dispersed nanofibers and porous structure (CMCP composites) possess larger surface areas and unique structural features to contribute to adsorbing proteins and increasing cell attachment, offering many more binding sites to cell membrane receptors, thereby providing far more conducive environments for the spread and proliferation of cells (Fig. 4c).

3.4. Self-expanding properties, dynamic expansion force and impact resistance

The CMCP showed fast liquid-triggered self-expanding ability and could deform from its initial shape to a highly expanded geometric shape in short times upon contacting liquid. After absorbing liquid, the CMCP exhibited considerable flexibility, stretchability and deformability (Fig. 5a). The volume expansion rate of the PVA and CMCPs were performed by immersing the materials in 37 °C PBS. As shown in Fig. 5a, the CMCP-2 and CMCP-3 could deform larger than 20× their original volumes during self-expansion. The volume expansion performance of CMCPs was significantly better than that of PVA, which could be resulted from the synergistic effect of the volumetric expansion of acetalized PVA and the swelling of CMC. The high volume expansion rate and deformability enabled small-sized CMCP to be directly sent to the bleeding site deep in wound cavity and instantly self-expand to more than 20× the original volume, thereby filling the entire cavity in seconds.

Important features required for materials used to treat serious bleeding or open wounds are the ability to generate assistant force to exert sufficient pressure to blood vessels and adequate strength to prevent the materials from dislocating from the wound site under rapid blood flow [42]. The dynamic expansion forces (DEF) generated by different materials during blood absorption are shown in Fig. 5b. Obviously, the expansion force of CMCPs greatly improved with increasing the CMC content. PVA exhibited the lowest DEF of less than 2 N, and the expansion force of CMCP-1 was twice this value. CMCP-3 possessed the largest DEF of 8 N, according to our previous analysis, this dynamic expansion force could produce a similar effect to manual pressing to exert sufficient pressure to surrounding tissues or blood vessels during the hemostatsis progress to help stop bleeding and prevent re-bleeding. It is worth mentioning that CMCP-2 and CMCP-3 required longer time (about 2 min) to reach the maximum expansion force. This is mainly due to that when contacting and absorbing the blood, these two composites had the ability to rapidly activate the coagulation system. Blood clots were continually formed on the surface and in the interior of the materials, which distinctly increased the actual measured expansion force. The magnitude of the expansion forces generated by CMCPs would not cause additional injury to the damaged

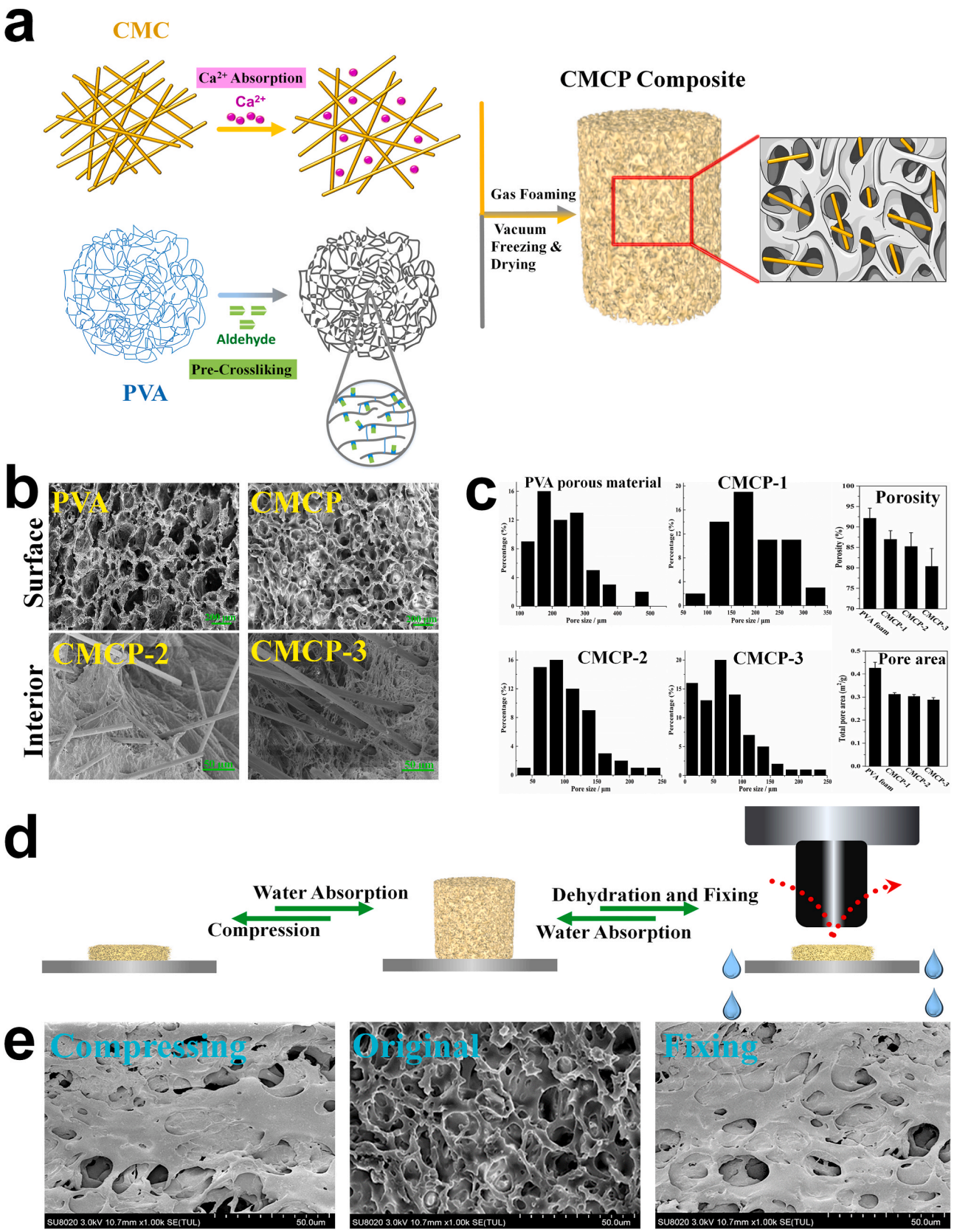

Fig. 3. **a**. Schematic diagram of the fabrication of the CMCP composites. **b**. SEM images of the morphology of the PVA porous materials and the CMCP composites. **c**. Pore size distribution, porosity and total pore area of different materials. **d**. The schematic representation of the liquid-triggered self-expand mechanism. **e**. Surface morphology of CMCP in compressed state, original state and shape-fixed state.

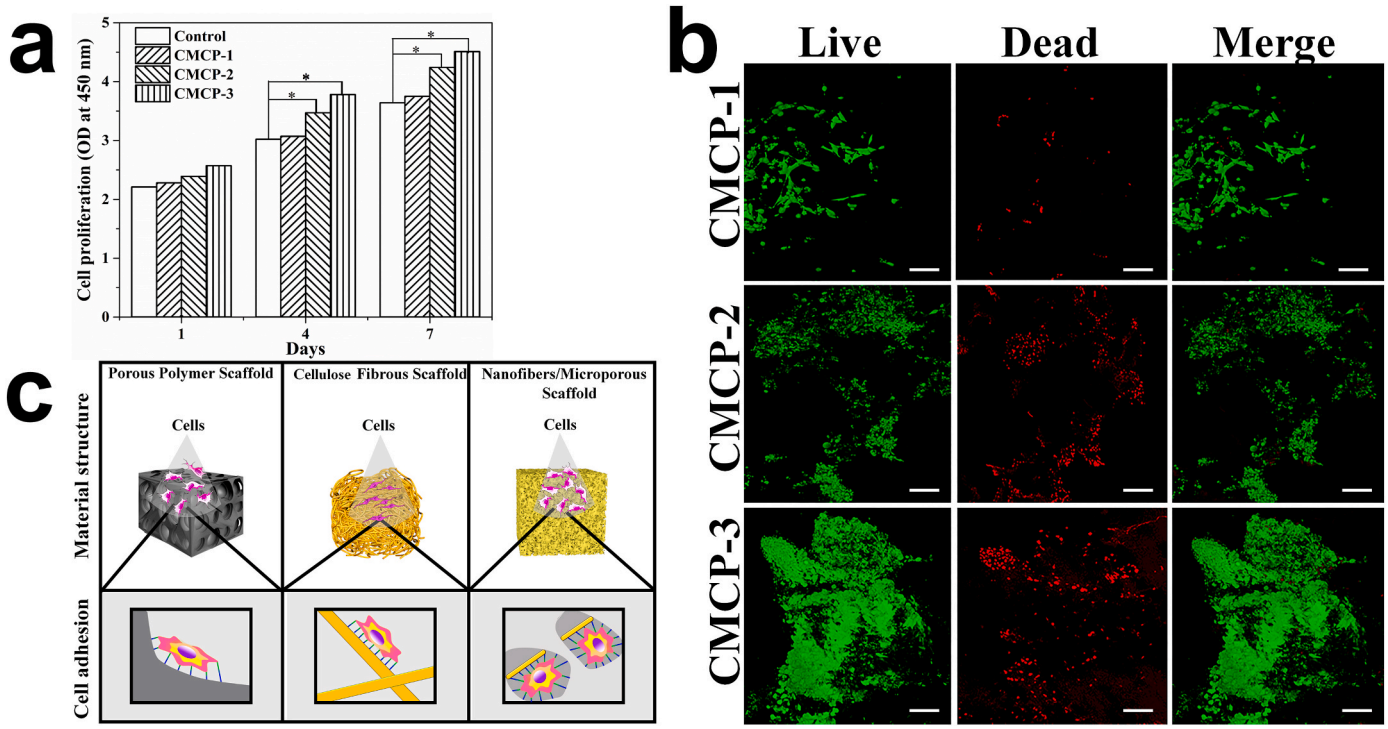

Fig. 4. **a**. The cytotoxicity of CMCP composites with different CMC content. (n = 3 per group). Error bars, mean ± s.d. (*p < 0.05, represents significant difference compared with control group). **b**. Live-Dead staining of L929 cells seeded on the surface of different composites after culturing for 7 days. Live cells emit green fluorescence, while dead cells emit red fluorescence. Scale bars: 100 μm. **c**. Effects of different material structures on cell binding and spreading.

tissue during application.

Rapid hemostasis for materials used for uncontrollable bleeding requires fast blocking of wound under continuous blood flow and sufficient mechanical strength to maintain blood pressure. Anti-impact stress test was therefore carried out to investigate the capacity of materials to withstand arterial blood pressure (Fig. 5c). Among all materials, medical gauze could withstand the smallest stress, 0.004 MPa. Porous PVA could withstand a slightly higher stress (0.018 MPa) than medical gauze, but it still could not meet the requirements for the treatment of arterial heavy bleeding. Instead, the anti-impact stress of CMCP composites was significantly improved, and the maximum stress that CMCP-2 and CMCP-3 composites could withstand were 0.083 MPa and 0.063 MPa, respectively, which were much higher than the arterial blood pressure in most clinical environments (systolic blood pressure 60–160 mmHg, 0.008–0.021 MPa). Therefore, we conclude that when the composite was used for treating massive hemorrhage, it had sufficient strength and could bear enough impulsive force to block the wound cavity and prevent blood from further flowing out, without causing its structural collapse or dislocation under blood pressure.

3.5. *Water absorption capacity and mechanical strength of the composites*

PVA showed better water absorption capacity with higher water content and water absorption rate than the CMCPs. For CMCPs, the water absorption capacity slightly decreased with increasing CMC content, which was probably due to the formation of more compact fiber-interspersed porous network, delaying or preventing the water from entering the composites (Fig. 5d). The results indicated that although the relative water absorption of the CMCP decreased compared with porous PVA, the CMCP was still able to absorb up to at least 13 times its dry weight in water within 40 s, which could definitely contribute to achieving rapid absorption of heavy bleeding at wound site [43].

Typical tensile stress-strain curves of the composites are shown in Fig. 5e. The tensile strength and elongation at break reflect the stiffness and tenacity of the materials, respectively. Compared with porous PVA, the CMCP composites had higher breaking strength, which significantly improved along with the increase of CMC content. The tensile stress-strain curve of porous PVA showed typical elastic deformation, while lots of irregular fluctuations were found on the curve of CMCP-1 during the tensile progress, which indicated that CMC was not uniformly distributed in CMCP-1. CMCP-2 and CMCP-3 maintained elastic deformation during tensile progress, and fluctuations only occurred on both curves when the composites started to break, demonstrating that CMC was evenly distributed in CMCP-2 and CMCP-3, and contributed to improving the breaking strength and mechanical stability of the composites.

Ideal hemostatic materials should have sufficient compressive strength to form physically barriers that work like stable hemostatic plugs at the wound site, to help block the wound and stop bleeding. On the other hand, high compressive and fatigue strength are also very essential for materials to generate assistant pressure to achieve hemostasis while avoiding structural collapse. Hence, as hemostatic materials, CMCP composites should bear a high enough stress while maintaining their structural stability during use, to generate efficient and continuous hemostatic effects on heavy and high-pressure bleeding. Systematical compression tests were carried out to evaluate the overall compressive properties and fatigue resistance of the composites. Fig. 5f shows the significant fiber reinforcement effects of CMC on CMCPs and the high compressive strength of the composites. The compression stress-strain curves of the materials after 50 cycles at the strain of 40%, 60% and 80%, respectively, were also drawn in Fig. 5(g–i). All the compressed porous materials could immediately recover their original shapes but exhibited slight plastic deformations under low compression strains (40% or below), and resilience loss of the CMCPs (CMCP-1, 8.4%; CMCP-2, 7.9%; CMCP-3, 8.3%) was significantly lower than that of porous PVA (11.2%). When the compression deformation increased to 80%, the CMCPs showed high fatigue resistance and no obvious resilience loss. After going through multiple compression cycles at high strain, the CMCPs maintained the volumes almost the same as their original volumes and their compression resilience remained well preserved.

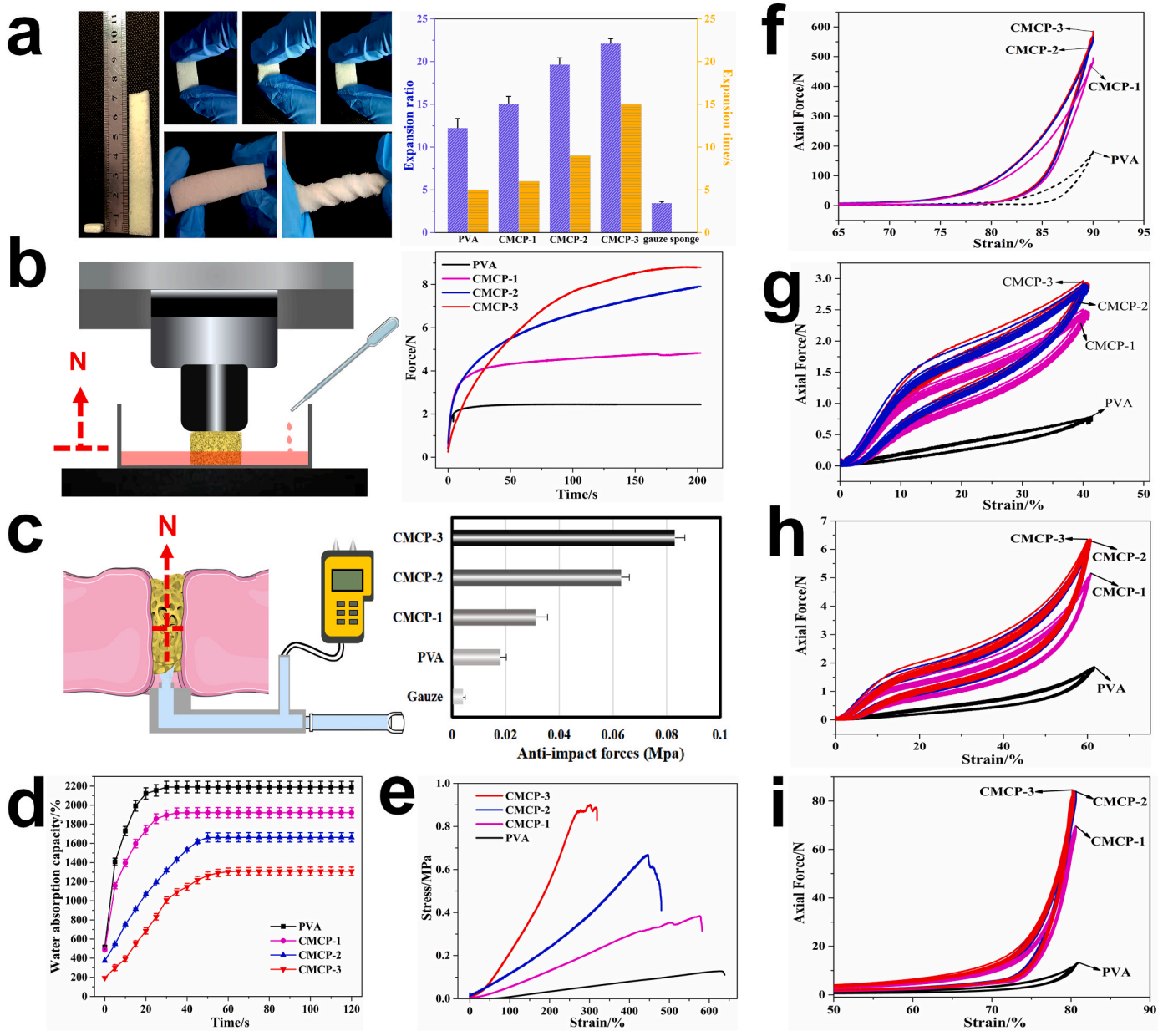

Fig. 5. **a**. The macroscopic images of CMCP before and after absorbing liquid, and the compression resistance capability, flexibility, deformable ability and expansion performance of the CMCP in wet state. **b**. The illustration of the dynamic expansion force test and the changes in expansion forces of different materials during the blood absorption progress. **c**. Schematic diagram of anti-impact test and the corresponding anti-impact stress of different materials. Water absorbing capacity (**d**) and tensile property (**e**) of different materials. Axial forces of different composites when bearing a 90% compression strain (**f**), and the cycling compressive curves (50 cycles) of different composites with strains of 40% (**g**), 60% (**h**) and 80% (**i**), respectively.

3.6. Protein absorption, blood cells adhesion and activation

SEM images of CMCP during fibrin absorption process are shown in Fig. 6a. Owing to the unique network structure and strong adsorption capacity, a large amount of fibrin could be adsorbed on the surface of CMCP. Meanwhile, with the extension of absorption time, dispersed protein particles gradually covered the surface of the composite, and gathered from irregular particles to fibrin network. After a long period of protein adsorption, a large number of protein particles could be observed entering the interior and attached to the fibrous network of the composite. The results demonstrated that the CMCP exhibited strong protein absorption capacity, which contributed to promoting the adhesion of blood cells and the rapid formation of stable clots on the composite.

Further, after interacted with PRP, large quantities of platelets were observed adhered to the surface of CMCP. In particular, more platelets adhered on the composites with higher CMC content, suggesting that the introduction of CMC improved the ability of CMCP to induce platelet aggregation (Fig. 6e). SEM images also showed that, with increasing time, plenty of activated and shape-changed platelets were found on the surface of CMCP composite, most of which extended "pseudopodia" (Fig. 6b). The effect of CMCP on red blood cells (RBCs) adhesion was then evaluated by quantitatively measuring the absorbance of hemoglobin. Materials with lower hemoglobin absorbance value indicated higher capability to trapping RBCs [44]. The results showed that the absorbance value of CMCPs group was significantly lower than that of PVA and blank group, and the absorbance value of CMCP-2 group was the lowest, indicating that CMCP-2 had the best ability to promote the

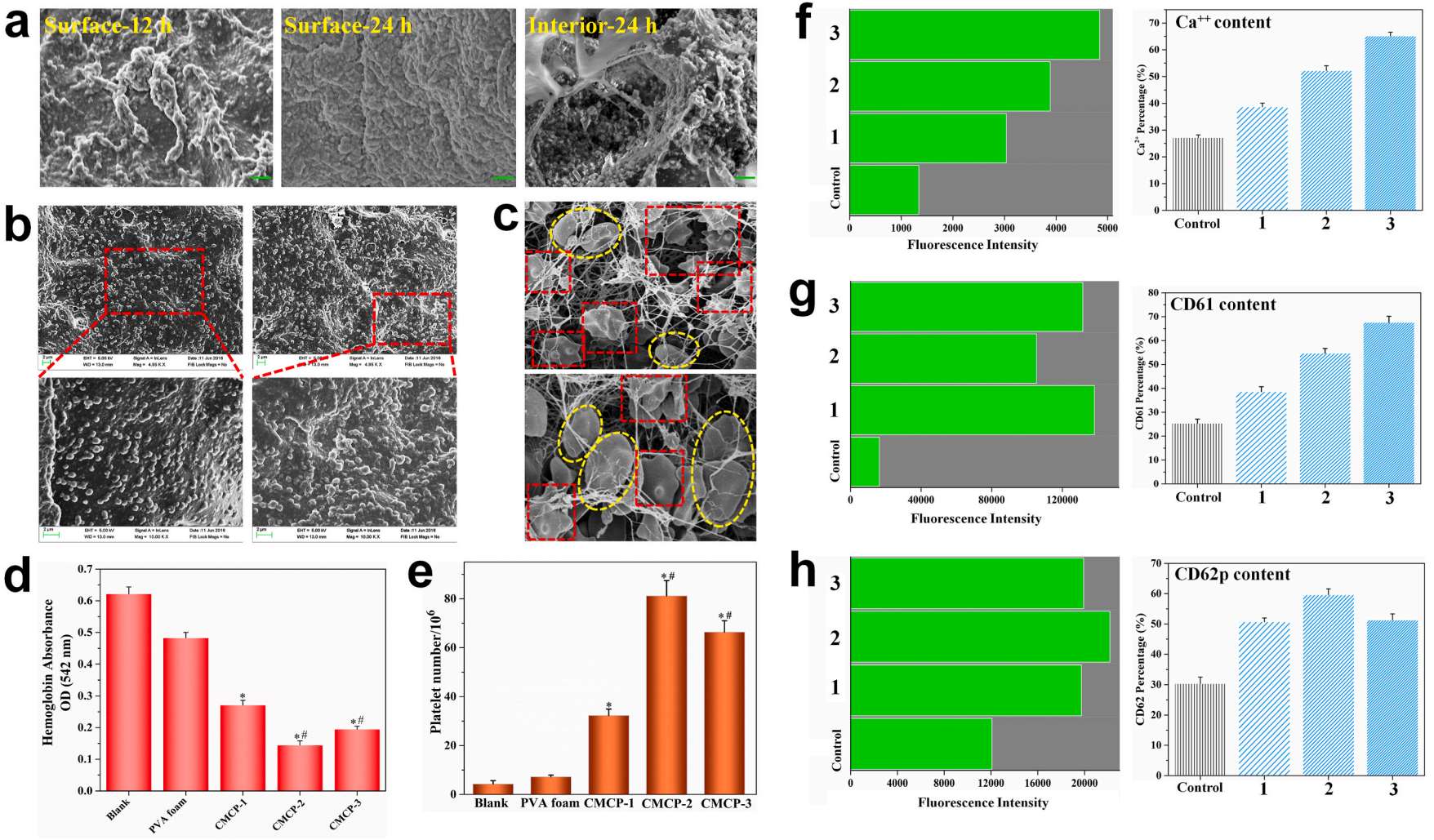

Fig. 6. **a**. SEM images of CMCP after absorbing protein. Scale bars: 2 μm. **b**. Measurement of the number of platelets adhered on different materials. **c**. SEM images of the adhered and activated platelets on the composite. **d**. The absorbance of the hemoglobin-containing solution. **e**. Blood cells adhesion (platelets and RBCs), platelets activation, and fibrin network formed and trapped blood cells. Yellow dotted circles indicate the RBCs, red dotted rectangles indicate the activated platelets. $^{*}p < 0.05$ and $^{\#}p < 0.05$ represent significant difference compared with the blank group. **f**, **g**, **h**. The fluorescence intensity and relative content of $Ca2^{+}$ in platelets, CD61 and CD62p were measured to evaluate the stimulating effects of CMCP on platelets.

RBCs adhesion (Fig. 6d). Considering that blood is in direct contact with the material during hemostasis, fresh blood was added directly to the surface of CMCP to investigate the interaction between material and blood components. As shown in Fig. 6c, the adhered blood cells were observed covered with large amounts of filamentous fibrin. After platelets and RBCs (yellow circles) adhered to the surface of CMCP, platelets were activated (red rectangles) by the porous structure and the negative charges. The activated platelets then triggered the production of thrombin, and the generated thrombin further promoted fibrin formation. Subsequently, the fibrin self-crosslinked to form a stable network and covered the adhered blood cells. All the above results demonstrated that the fiber-interspersed porous structure greatly increased the surface area and surface roughness of the CMC, enabling the blood cells to rapidly adhere on it. In addition, the dispersed and immobilized CMC fibers in the CMCP matrix would allow large numbers of carboxymethyl groups with negative charges to be exposed to blood, thereby inducing the activation and aggregation of platelets and activating the intrinsic pathway of coagulation cascade. Combined with previous results, the ability of CMCP to promote blood clotting could be attributed to its high adhesion to protein and blood cells as well as ability to accelerate the activation of platelets.

To verify this conclusion, the concentrations of intracellular Ca^{2+}, P-selectin and CD61 were determined to evaluate the activating effects of the CMCP on platelets. Ca^{2+} plays an important role in regulating the physiological activities of platelets and the concentration of free Ca^{2+} in platelets also has important impacts on the aggregation, activation and degeneration of platelets [45]. Intracellular signaling, which depends on Ca^{2+} in the cytoplasm, can trigger a structural change in GPIIbIIIa, and induce the aggregation of fibrinogen-mediated platelets [46]. Therefore, the changes of Ca^{2+} concentration in platelets could reflect the effects of materials on the physiological activities of platelets. Fig. 6f shows the FI of the intracellular Ca^{2+} after treated with different materials. The content (Ca^{2+} percentage in platelets) and FI of Ca^{2+} of CMCPs groups gradually increased with the increasing CMC content, and were significantly higher than those of the control group. Generally, increased Ca^{2+} concentration in platelets can trigger the activation of integrin and eventually lead to the aggregation of platelets. Therefore, we concluded that CMCP composite had a significant effect on the changes of intracellular Ca^{2+} concentration in the platelet, and could efficiently promote the aggregation and activation of platelets.

CD61 (GPIIIa) is a glycoprotein found on platelets or along with the alpha IIb chain in platelets, which plays a vital role in platelet aggregation. Like other integrins, CD61 generally takes part in cell-surface mediated signaling and cell adhesion. CD62p (P-selectin) is a transmembrane glycoprotein and stored in α-granules of platelets [47]. CD62p redistributes to the plasma membrane during platelet activation and mediates activated platelets adhesion and stretching [48]. Once platelets are activated, the release and expression of CD61 and P-selectin will be enhanced remarkably. Therefore, the effect of CMCP on the stimulation and activation platelet can be assessed by measuring the FI and relative content of CD61 and CD62p. As shown in Fig. 6g and h, the FI and relative content of P-selectin and CD61 of CMCPs groups were significantly increased compared with that of blank group, indicating that CMCP composite could stimulate a large release of CD61 and CD62p, and thus significantly promote the aggregation and activation of platelets. This result in combination with the previous result of changes in Ca^{2+} concentration in platelets, indicated that the CMCP could not only promote the adhesion and aggregation of blood cells, but also accelerate the coagulation process by activating platelets.

3.7. *In vivo* hemostatic performance

To evaluate the clinical hemostatic efficacy of CMCP composite, a femoral artery injury model of pigs was then employed. CMCP-2 samples were selected for *in vivo* hemostasis study because of its favorable structural properties and excellent *in vitro* coagulation properties. The

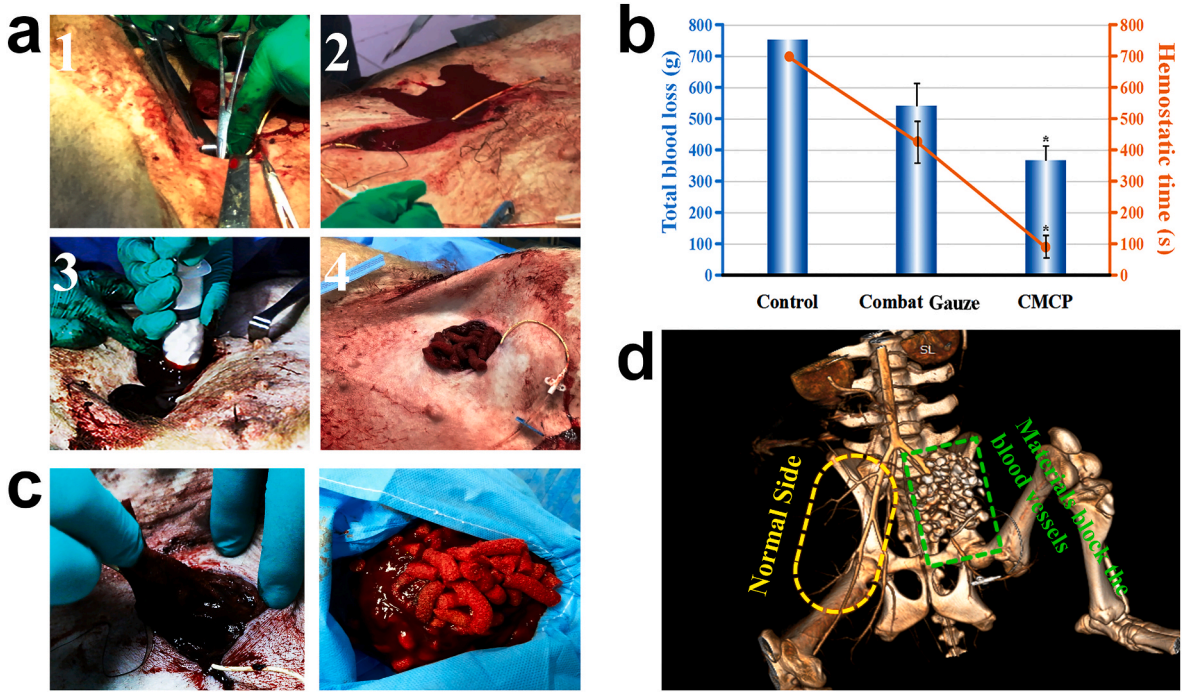

Fig. 7. Evaluation of hemostatic performance of CMCP in a swine femoral artery injury model. **a**. The femoral artery of the anesthetized swine was first exposed and then severed to make lethal blood loss. After free bleeding for 30 s, the cylindrical CMCP particles were immediately injected into the wound, and hemostasis was achieved in short times. **b**. Total blood loss and hemostatic time. Control group: Manual pressure. In the control group, the shortest hemostatic time of experimental animals was longer than 700 s, and some of the animals (n = 3) failed to achieve hemostasis during the experiment. *p < 0.05 represent significant difference compared with Combat Gauze group. **c**. Removal of samples from the wound after hemostasis. **d**. CT angiography image of blood vessels and blood flow after CMCP treatment.

femoral artery was completely exposed and transected using surgical scissors, and CMCP samples were injected to fill the wound cavity as quickly as possible using an injector with diameter of 3 cm to enable their full contacting with the bleeding site (Fig. 7a). In the other experiment group, Combat Gauze (Z-Medica), which is a kaolin impregnated gauze [29], was directly packed into the wound. Continuously manual press was used in control group. The control group failed to achieve hemostasis within 10 min (n = 4). Compared with the Combat Gauze group (n = 4), the CMCP group had shorter hemostatic time and less blood loss (n = 4), demonstrating that the CMCP composite had better hemostatic capacity. (Fig. 7b). No pigs were died during and after the operation in the CMCP group. After hemostasis achieved, the composite samples were removed from the wound cavity, and large amount of blood clots were found formed on the surface or in the interior of the composite. More importantly, during the hemostasis process, the samples were observed clustered together via greatly concentrating the blood component and forming large number of clots surrounded them, and all samples were integrated by the formed blood clots, which facilitated the subsequent removal of the samples and preoperative debridement (Fig. 7c). Angiography was then employed to detect the blood vessels and blood flow in tissues after hemostasis. The green rectangle on the right showed the injury site, and the yellow ellipse denoted the corresponding part in normal tissue. On the normal side, all the blood vessels are clear and continuous, and no breakpoints or blockages were observed. Compared with the normal side, the severed femoral artery and surrounding vessels on the other side had been completely blocked by the CMCP samples, and all the samples were found located in the wound cavity and did not enter the blood vessels or disperse to other parts of animal body. Besides, the walls of all blood vessels at the bleeding site were smooth, indicating that CMCP did not cause thrombosis in vessels.

3.8. Shape-adaptive ability of composites to wound tissues

For narrow, deep or irregular wounds, in addition to injectable particle samples, we also designed polygonal stick samples. The samples with different shapes were further used to fill the unique-shaped femoral artery wound cavities designed by surgery, to visually observe the hemostatic efficacy and self-expanding properties and the shape adaptability of the CMCP. An appropriate amount of contrast agent was first combined with CMCP samples and uniformly distributed in the composite. As shown in Fig. 8a, the physicochemical performance of the CMCP, especially the self-expanding properties and the liquid absorption capacity, remained unchanged after incorporating the contrast agent. A pre-experiment was carried out using only animal tissues. As shown in the CT images, after the small-sized CMCP samples were crammed into tissue cavity, they rapidly self-expanded through contacting blood, filled entire irregular-shaped cavity and achieved shape-adaptive to the irregular tissues (Fig. 8b).

Two kinds of CMCP samples with different shape (particles and sticks) were applied to unique-shaped wound cavities made by surgery. *In vivo* hemostasis test found that these two kinds of samples both exhibited excellent hemostatic efficacy on large artery hemorrhage (Fig. 8c). Subsequently, CT tomography and 3D reconstruction were

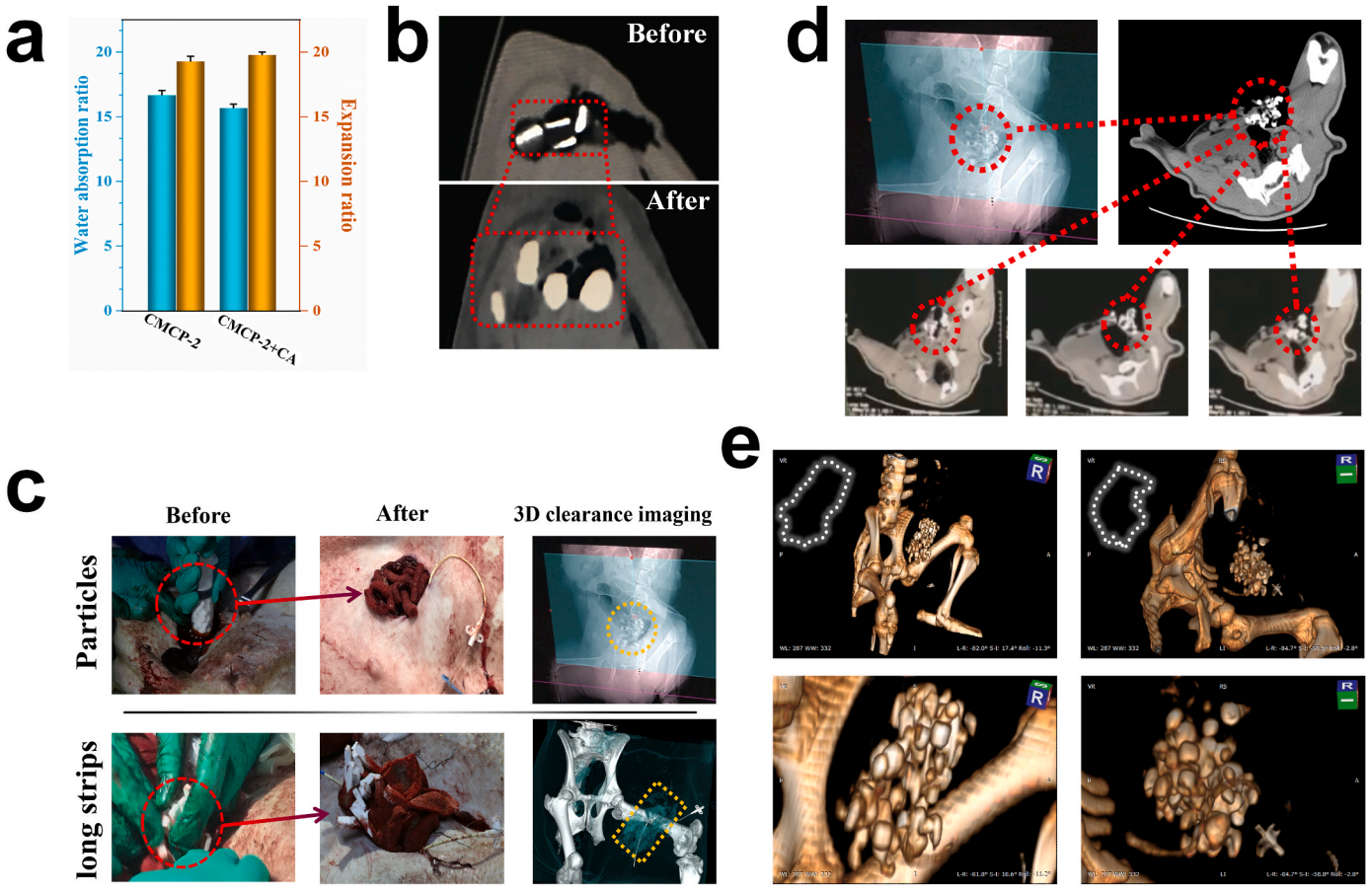

Fig. 8. **a**. The changes of the water absorption and expansion properties of the CMCP before and after incorporating contrast agent. **b**. Pre-experiment was used to observe the changes of the morphology and position of the CMCP particles during the blood-absorbing process in the tissue cavity. **c**. Two kinds of CMCP samples with different shapes (particles and sticks) were applied to the femoral artery injury wound. **d**. The shape-adaptive ability of the CMCP to the surrounding tissues at different depths in wound cavity. **e**. Shape-adaptive ability of CMCPs to the wound cavities with different shapes. The white dotted curves represent the shapes of the wound cavities.

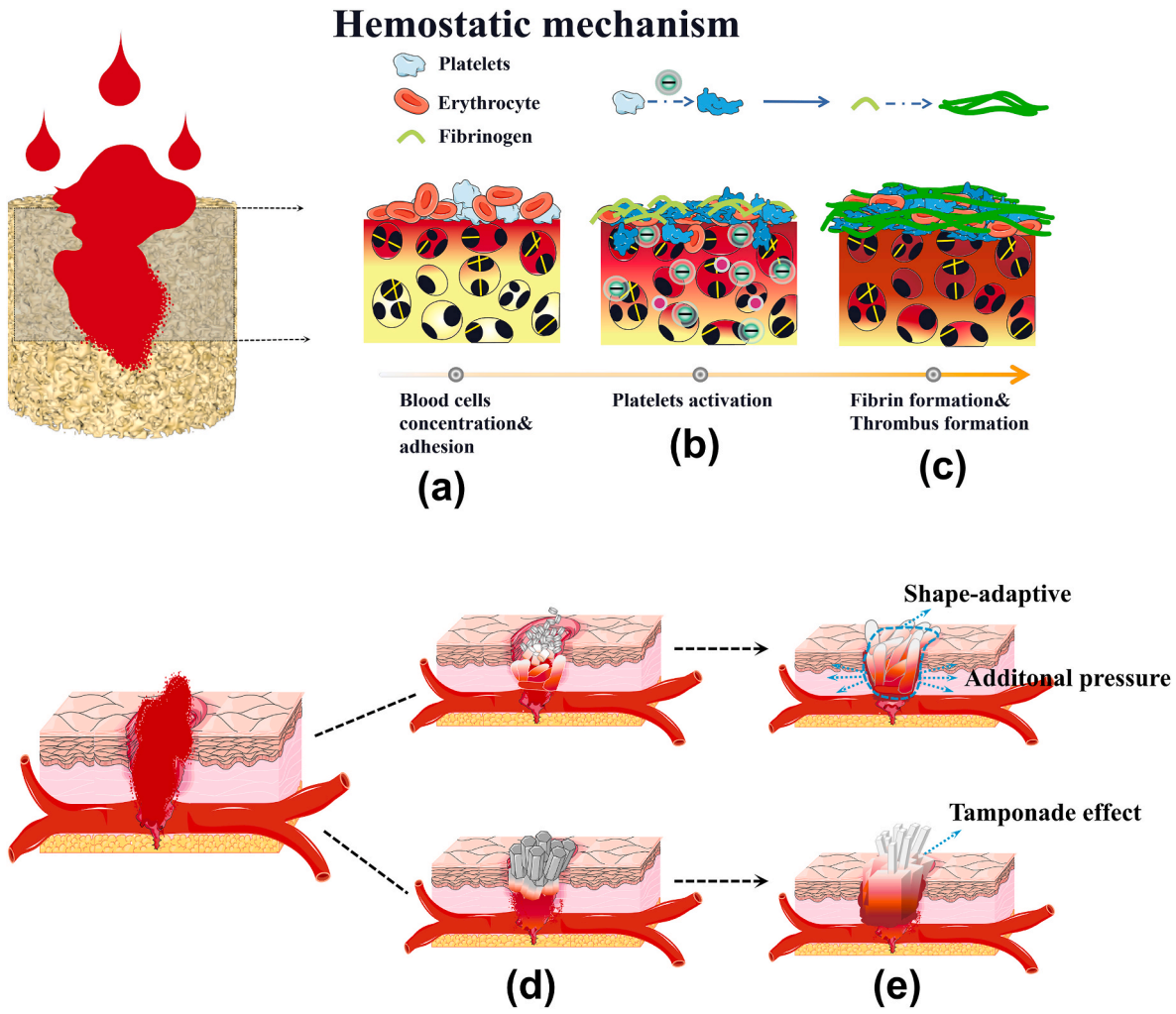

Fig. 9. Multiple mechanisms of CMCP synergistically promote the hemostasis. **a**. CMCP rapidly absorbed blood, trapped and concentrate blood cells by its fiber-interspersed porous network. **b**. Adhered platelets and blood clotting factors were activated by CMCP. **c**. Rapid formation of stable thrombus. **d**. CMCP samples were made into different shapes for the treatment of arterial bleeding. **e**. CMCP absorbed blood and self-expanded, blocked the wound through the tamponade effect, exerted auxiliary pressure on surrounding tissues and vessels, and finally completely fitted the shape of wound cavity through shape-adaptive ability to achieve hemostasis.

used to observe the shape-adaptability of CMCP to the cavity with specific shapes. As shown in the 3D imaging based on cavity gap, both the two different shaped samples completely filled the wound cavity and blocked the wound, and the shape adaptability was independent of the shape and size of the materials. Furthermore, it could be observed from the CT images that the samples could achieve shape-adaptive to the surrounding tissues at different depths in the wound cavity (Fig. 8d). Meanwhile, 3D reconstruction showed that when used to treat wounds of different sizes and shapes, during the hemostasis process, the CMCP samples with good flexibility and deformability could gather together through blood-triggered self-expansion to form exactly the same shape as the wound cavities, achieving shape-adaptation to both the surrounding tissues and wound cavity (Fig. 8e). Besides, CMCP could adaptively change its shape to better fit the adjacent tissues inside the wound and fully fill the wound lacunae or wound tract, which could contribute to effectively compressing the vessels, inhibiting bleeding and preventing infection. The results of CT tomography and 3D reconstruction demonstrated that the CMCP could be delivered into deep, irregular or massive bleeding wound, and would rapidly absorb blood and immediately undergo self-expansion to fill the entire wound cavity and achieve the shape-adaption to wound tissues.

3.9. Hemostatic mechanism

Fig. 9 shows that multiple mechanisms in CMCP acted synergistically to promote hemostasis. The rapid and effective hemostatic mechanism of CMCP can be attributed to the following five aspects:

(I) Blood cell concentration: CMCP composite could rapidly absorb blood, allowing the aggregation of blood cells. Meanwhile, the unique fiber-interspersed porous network structure of CMCP is also advantageous to trap blood cells and promote the adhesion of blood cells, thereby activating the coagulation system.

(II) Stimulation of negative charges and Ca^{2+}: After contacting with blood, the Ca^{2+} and carboxyl groups on the CMC could be fully exposed to the blood, which is beneficial to activate platelets and coagulation factors in the blood, and promote the formation of stable thrombus inside and on the surface of the CMCP.

(III) Tamponade effects: The introduction of CMC improves the toughness, mechanical strength and fatigue resistance of CMCP composites. This ensures that the CMCP would not break or dislocate in the wound cavity under the blood pressure and blood flow, and could completely block the wound, achieving the tamponade effect similar to medical gauze or sponge.

(IV) Assisted pressure: CMCP possessed the ability of blood-triggered rapid self-expansion, and could generate long-term stable dynamic force during expansion. This dynamic expansion force provides additional stress which was similar to manual compression on surrounding tissues or blood vessels, and helps to mechanically achieve hemostasis.

(V) Shape-adaptive ability: CMCP with high flexibility and deformability can achieve shape adaptive to any shape and size of tissue cavity. This unique ability allowed CMCP to be delivered to irregular, narrow or deep wounds in a very small size, and rapidly undergo self-expansion through contacting blood to completely attach to the wound tissue, effectively stopping bleeding, protecting wound tissue and preventing infection.

Most of the hemostats currently used in medical care or military, such as gauze, chitosan hemostatic agents, zeolite and montmorillonite, usually work only through one single hemostatic mechanism, and thus exhibit low hemostatic efficacy for wounds in the groin or armpit, firearm or penetrating injury, which cannot meet the pre-hospital first-aid treatment. Meanwhile, in recent years, plenty of experimental hemostatic materials have been developed and used for rapid wound sealing and bleeding control, including sponges or foams, microspheres or beads, gauzes or zeolites, and functional hydrogels [49,50]. Previous studies have proven that some of these materials show the ability to control mild bleeding of artery or heart and promote wound healing [34,51]. However, because of slow hemostatic performance, low hemostatic efficacy, poor mechanical strength and flexibility, these hemostats are ineffective or unsuitable for treating aortic trauma or large/irregular wounds. Additionally, most of them are effective only for mild to moderate bleeding. Therefore, the investigation of CMCP with excellent biological safety and multiple hemostatic effects is of great significance for the treatment of uncontrollable hemorrhage caused by war injuries, natural disasters or accidents, and will also provide ideas for the R&D efforts of new convenient and efficient low-cost hemostatic materials.

4. Conclusions

In this work, carboxymethyl cellulose fibers with high water absorption, high substitution degree and hemostatic ability were first prepared and a series of composites with unique fibers-interspersed porous network structure was subsequently developed. The composites exhibited favorable physicochemical performance, good biocompatibility and blood compatibility. Furthermore, owing to their high blood absorption and blood cells adhesion, and powerful capacity to activate the coagulation system and promote thrombus formation, the CMCP composites were efficient for blood clotting and presented strong hemostatic efficacy in a swine femoral artery injury model. More importantly, the liquid-triggered self-expanding property endowed the CMCP with fast and specific shape-adaptive ability to irregular and deep wound cavity, and the force generated by self-expansion could also contribute to exerting assistant pressure on surrounding tissues to accelerate hemostasis. All these results demonstrated that CMCP with multiple hemostatic mechanisms will be a promising hemostat for controlling severe hemorrhage and treating narrow, irregular or deep wounds, and will also greatly promote the development of hemostasic technologies in the field of military or civilian trauma.

CRediT authorship contribution statement

Yansen Wang: Conceptualization, Investigation, Methodology, Writing-Original draft. **Yifan Zhao:** Methodology, Investigation. **Longxue Qiao:** Investigation. **Faxing Zou:** Visualization, Data curation. **Yajie Xie:** Investigation. **Yudong Zheng:** Resources, Supervision, Validation. **Yong Chao:** Resources, Supervision, Validation. **Ying Yang:** Investigation. **Wei He:** Writing-Review&Editing. **Siming Yang:** Resources, Supervision, Validation.

Declaration of competing interest

There are no conflict of interest for our manuscript.

Acknowledgements

This work is financially supported by National Natural Science Foundation of China (Nos. 51773018, 51973018 and 31700829) and Key Research and Development Projects of People's Liberation Army (BWS17J036).

Appendix A. Supplementary data

Supplementary data to this article can be found online at https://doi.org/10.1016/j.bioactmat.2020.12.014.

References

[1] Emma Marris, Four years in Iraq: the war against wounds, Nature 446 (7134) (2007) 369–371, https://doi.org/10.1038/446369a.
[2] R. Lozano, M. Naghavi, K.J. Foreman, S.S. Lim, K. Shibuya, V. Aboyans, J. P. Abraham, T. Adair, R. Aggarwal, S.Y. Ahn, Global and regional mortality from 235 causes of death for 20 age groups in 1990 and 2010: a systematic analysis for the Global Burden of Disease Study 2010, Lancet 380 (9859) (2012) 2095–2128, https://doi.org/10.1016/S0140-6736(12)61728-0.
[3] W. Leslie, Chae Chan, Kim Hwa, Wang Xu, H. Suzie, PolySTAT-modified chitosan gauzes for improved hemostasis in external hemorrhage, Acta Biomater. 31 (2016) 178–185, https://doi.org/10.1016/j.actbio.2015.11.017.
[4] J. Wen, M. Weinhart, B. Lai, J.N. Kizhakkedathu, D.E. Brooks, Reversible hemostatic properties of sulfabetaine/quaternary ammonium modified hyperbranched polyglycerol, Biomaterials 86 (2016) 42–55, https://doi.org/10.1016/j.biomaterials.2016.01.067.
[5] A.M. Behrens, M.J. Sikorski, P. Kofinas, Hemostatic strategies for traumatic and surgical bleeding, J. Biomed. Mater. Res. 102 (11) (2014) 4182–4194, https://doi.org/10.1002/jbm.a.35052.
[6] M.A. Boerman, E. Roozen, M.J. Sanchezfernandez, A.R. Keereweer, R.P.F. Lanao, J. C.M.E. Bender, R. Hoogenboom, S.C.G. Leeuwenburgh, J.A. Jansen, H. Van Goor, Next generation hemostatic materials based on NHS-ester functionalized poly(2-oxazoline)s, Biomacromolecules 18 (8) (2017) 2529–2538, https://doi.org/10.1021/acs.biomac.7b00683.
[7] N.R. Kunio, G.M. Riha, K.M. Watson, J.A. Differding, M.A. Schreiber, J.M. Watters, Chitosan based advanced hemostatic dressing is associated with decreased blood loss in a swine uncontrolled hemorrhage model, Am. J. Surg. 205 (5) (2013) 505–510, https://doi.org/10.1016/j.amjsurg.2013.01.014.
[8] M. Pozza, R.W.J. Millner, Celox (chitosan) for haemostasis in massive traumatic bleeding, Eur. J. Emerg. Med. 18 (1) (2011) 31–33, https://doi.org/10.1097/MEJ.0b013e32833a5ee4.
[9] B.L. Bennett, L.F. Littlejohn, Review of new topical hemostatic dressings for Combat casualty care, Mil. Med. 179 (5) (2014) 497–514, https://doi.org/10.7205/MILMED-D-13-00199.
[10] J. John, Devlin, Kircher Sara, G. Buddy, Kozen, comparison of ChitoFlex®, CELOX™, and QuikClot® in control of hemorrhage, J. Emerg. Med. 41 (2011) 237–245, https://doi.org/10.1016/j.jemermed.2009.02.017.
[11] G. Buddy, Kozen, J. Sara, Jose Kircher, Henao, S. Fermin, An alternative hemostatic dressing: comparison of CELOX, HemCon, and QuikClot, Acad. Emerg. Med. 15 (2008) 74–81, https://doi.org/10.1111/j.1553-2712.2007.00009.x.
[12] Y. Liang, C. Xu, F. Liu, S. Du, G. Li, X. Wang, Eliminating heat injury of zeolite in hemostasis via thermal conductivity of graphene sponge, ACS Appl. Mater. Interfaces 11 (27) (2019) 23848–23857, https://doi.org/10.1021/acsami.9b04956.
[13] T.R. Muench, W. Kong, A.M. Harmon, The performance of a hemostatic agent based on oxidized regenerated cellulose – polyglactin 910 composite in a liver defect model in immunocompetent and athymic rats, Biomaterials 31 (13) (2010) 3649–3656, https://doi.org/10.1016/j.biomaterials.2010.01.070.
[14] L. Zhang, H. Ge, M. Xu, J. Cao, Y. Dai, Physicochemical properties, antioxidant and antibacterial activities of dialdehyde microcrystalline cellulose, Cellulose 24 (5) (2017) 2287–2298, https://doi.org/10.1007/s10570-017-1255-4.
[15] C. Chen, H. Li, J. Pan, Z. Yan, Z. Yao, W. Fan, C. Guo, Biodegradable composite scaffolds of bioactive glass/chitosan/carboxymethyl cellulose for hemostatic and bone regeneration, Biotechnol. Lett. 37 (2) (2015) 457–465, https://doi.org/10.1007/s10529-014-1697-9.
[16] K.M. Lewis, D. Spazierer, M.D. Urban, L. Lin, H. Redl, A. Goppelt, Comparison of regenerated and non-regenerated oxidized cellulose hemostatic agents, European Surgery-acta Chirurgica Austriaca 45 (4) (2013) 213–220, https://doi.org/10.1007/s10353-013-0222-z.
[17] S.D. Dimitrijevich, M. Tatarko, R.W. Gracy, G.E. Wise, L.X. Oakford, C.B. Linsky, L. Kamp, In vivo degradation of oxidized, regenerated cellulose, Carbohydr. Res. 198 (2) (1990) 331–341, https://doi.org/10.1016/0008-6215(90)84303-C.
[18] D.A. Hickman, C.L. Pawlowski, U.D.S. Sekhon, J. Marks, A.S. Gupta, Biomaterials and advanced technologies for hemostatic management of bleeding, Adv. Mater. 30 (4) (2018) 1700859, https://doi.org/10.1002/adma.201700859.

[19] H. Yuan, L. Chen, F. Hong, A biodegradable antibacterial nanocomposite based on oxidized bacterial nanocellulose for rapid hemostasis and wound healing, ACS Appl. Mater. Interfaces 12 (3) (2020) 3382–3392, https://doi.org/10.1021/acsami.9b17732.
[20] Q. Yu, Y. Zheng, N. Yan, Y. Xie, K. Qiao, R. Jin, The gelation process and protein absorption property of injectable SA-CMBC hydrogel used for procoagulant material, RSC Adv. 5 (129) (2015) 106953–106958, https://doi.org/10.1039/C5RA19562D.
[21] M.E. Davis, Ordered porous materials for emerging applications, Nature 417 (6891) (2002) 813–821, https://doi.org/10.1002/chin.200240245.
[22] K. Quan, G. Li, D. Luan, Q. Yuan, L. Tao, X. Wang, Black hemostatic sponge based on facile prepared cross-linked graphene, Colloids Surf. B Biointerfaces 132 (2015) 27–33, https://doi.org/10.1016/j.colsurfb.2015.04.067.
[23] G. Li, K. Quan, Y. Liang, T. Li, Q. Yuan, L. Tao, Q. Xie, X. Wang, Graphene-montmorillonite composite sponge for safe and effective hemostasis, ACS Appl. Mater. Interfaces 8 (51) (2016) 35071–35080, https://doi.org/10.1021/acsami.6b13302.
[24] K. Quan, G. Li, L. Tao, Q. Xie, Q. Yuan, X. Wang, Diaminopropionic acid reinforced graphene sponge and its use for hemostasis, ACS Appl. Mater. Interfaces 8 (12) (2016) 7666–7673, https://doi.org/10.1021/acsami.5b12715.
[25] G.R. Mueller, T. Pineda, H.X. Xie, J.S. Teach, A.D. Barofsky, J.R. Schmid, K. W. Gregory, A novel sponge-based wound stasis dressing to treat lethal noncompressible hemorrhage, J. Trauma Inj. Infect. Crit. Care 73 (2012) S134–S139, https://doi.org/10.1097/TA.0b013e3182617c3c.
[26] S.M. Stuart, G.J. Zarow, A.C. Walchak, J. Mclean, P.J.D. Roszko, Pilot study of a novel swine model for controlling junctional hemorrhage using the iTClamp in conjunction with hemostatic agents, Mil. Med. 184 (2019) 367–373, https://doi.org/10.1093/milmed/usy337.
[27] T.L. Landsman, T. Touchet, S.M. Hasan, C. Smith, B. Russell, J. Rivera, D. J. Maitland, E. Cosgriffhernandez, A shape memory foam composite with enhanced fluid uptake and bactericidal properties as a hemostatic agent, Acta Biomater. 47 (47) (2017) 91–99, https://doi.org/10.1016/j.actbio.2016.10.008.
[28] X. Liu, Y. Niu, K.C. Chen, S. Chen, Rapid hemostatic and mild polyurethane-urea foam wound dressing for promoting wound healing, Mater. Sci. Eng. C 71 (2017) 289–297, https://doi.org/10.1016/j.msec.2016.10.019.
[29] X. Zhao, B. Guo, H. Wu, Y. Liang, P.X. Ma, Injectable antibacterial conductive nanocomposite cryogels with rapid shape recovery for noncompressible hemorrhage and wound healing, Nat. Commun. 9 (1) (2018) 2784, https://doi.org/10.1038/s41467-018-04998-9.
[30] Y. Wang, C. Wang, L. Qiao, J. Feng, Y. Zheng, Y. Chao, W. He, Y. Xie, W. Shuai, M. Li, Shape-adaptive composite foams with high expansion and absorption used for massive hemorrhage control and irregular wound treatment, Applied Materials Today 13 (2018) 228–241, https://doi.org/10.1016/j.apmt.2018.09.009.
[31] H. Du, Y. Zheng, W. He, Y. Sun, Y. Wang, A novel expandable porous composite based on acetalized polyvinyl alcohol and calcium sulfate used for injectable bone repair materials, Compos. Sci. Technol. 157 (2018) 10–20, https://doi.org/10.1016/j.compscitech.2018.01.014.
[32] N.A. Batista, A.A. Rodrigues, V.P. Bavaresco, J.R.L. Mariolani, W.D. Belangero, Polyvinyl alcohol hydrogel irradiated and acetalized for osteochondral defect repair: mechanical, chemical, and histological evaluation after implantation in rat knees, International Journal of Biomaterials 2012 (2012) 582685, https://doi.org/10.1155/2012/582685.
[33] Y. Wang, Y. Zheng, W. He, C. Wang, Y. Sun, K. Qiao, X. Wang, L. Gao, Reprint of: preparation of a novel sodium alginate/polyvinyl formal composite with a double crosslinking interpenetrating network for multifunctional biomedical application, Compos. B Eng. 121 (2017) 9–22, https://doi.org/10.1016/j.compositesb.2017.01.045.
[34] Y. Hong, F. Zhou, Y. Hua, X. Zhang, C. Ni, D. Pan, Y. Zhang, D. Jiang, L. Yang, Q. Lin, A strongly adhesive hemostatic hydrogel for the repair of arterial and heart bleeds, Nat. Commun. 10 (1) (2019) 2060, https://doi.org/10.1038/s41467-019-10004-7.
[35] R. Gu, W. Sun, H. Zhou, Z. Wu, Z. Meng, X. Zhu, Q. Tang, J. Dong, G. Dou, The performance of a fly-larva shell-derived chitosan sponge as an absorbable surgical hemostatic agent, Biomaterials 31 (6) (2010) 1270–1277, https://doi.org/10.1016/j.biomaterials.2009.10.023.
[36] C.N. Sambasivan, S.D. Cho, K.A. Zink, J.A. Differding, M.A. Schreiber, A highly porous silica and chitosan-based hemostatic dressing is superior in controlling hemorrhage in a severe groin injury model in swine, Am. J. Surg. 197 (5) (2009) 576–580, https://doi.org/10.1016/j.amjsurg.2008.12.011.
[37] G.P. De Castro, M.B. Dowling, M. Kilbourne, K. Keledjian, I.R. Driscoll, S. R. Raghavan, J.R. Hess, T.M. Scalea, G.V. Bochicchio, Determination of efficacy of novel modified chitosan sponge dressing in a lethal arterial injury model in swine, J. Trauma Inj. Infect. Crit. Care 72 (4) (2012) 899–907, https://doi.org/10.1097/TA.0b013e318248baa1.
[38] L. Yue, Y. Zheng, Y. Xie, S. Liu, S. Guo, B. Yang, T. Tang, Preparation of a carboxymethylated bacterial cellulose/polyaniline composite gel membrane and its characterization, RSC Adv. 6 (73) (2016) 68599–68605, https://doi.org/10.1039/C6RA07646G.
[39] Q. Lin, Y. Zheng, L. Ren, J. Wu, H. Wang, J. An, W. Fan, Preparation and characteristic of a sodium alginate/carboxymethylated bacterial cellulose composite with a crosslinking semi-interpenetrating network, J. Appl. Polym. Sci. 131 (3) (2014) 39848, https://doi.org/10.1002/app.39848.
[40] X. Zhao, H. Wu, B. Guo, R. Dong, Y. Qiu, P.X. Ma, Antibacterial anti-oxidant electroactive injectable hydrogel as self-healing wound dressing with hemostasis and adhesiveness for cutaneous wound healing, Biomaterials 122 (2017) 34–47, https://doi.org/10.1016/j.biomaterials.2017.01.011.
[41] B. Blakeney, A. Tambralli, J.M. Anderson, A. Andukuri, D. Lim, D. Dean, H. Jun, Cell infiltration and growth in a low density, uncompressed three-dimensional electrospun nanofibrous scaffold, Biomaterials 32 (6) (2011) 1583–1590, https://doi.org/10.1016/j.biomaterials.2010.10.056.
[42] R. Imani, M. Rafienia, S.H. Emami, Synthesis and characterization of glutaraldehyde-based crosslinked gelatin as a local hemostat sponge in surgery: an in vitro study, Bio Med. Mater. Eng. 23 (3) (2013) 211–224, https://doi.org/10.3233/BME-130745.
[43] Y. Lyu, H. Ren, M. Yu, X. Li, D. Li, C. Mu, Using oxidized amylose as carrier of linalool for the development of antibacterial wound dressing, Carbohydr. Polym. 174 (2017) 1095–1105, https://doi.org/10.1016/j.carbpol.2017.07.033.
[44] P.T.S. Kumar, V. Lakshmanan, T.V. Anilkumar, C. Ramya, P. Reshmi, A. G. Unnikrishnan, S.V. Nair, R. Jayakumar, Flexible and microporous chitosan hydrogel/nano ZnO composite bandages for wound dressing: in vitro and in vivo evaluation, ACS Appl. Mater. Interfaces 4 (5) (2012) 2618–2629, https://doi.org/10.1021/am300292v.
[45] I. Jardin, J.J. Lopez, J.A. Pariente, G.M. Salido, J.A. Rosado, Intracellular calcium release from human platelets: different messengers for multiple stores, Trends Cardiovasc. Med. 18 (2) (2008) 57–61, https://doi.org/10.1016/j.tcm.2007.12.004.
[46] Z. Chen, X. Yao, L. Liu, J. Guan, M. Liu, Z. Li, J. Yang, S. Huang, J. Wu, F. Tian, Blood coagulation evaluation of N-alkylated chitosan, Carbohydr. Polym. 173 (2017) 259–268, https://doi.org/10.1016/j.carbpol.2017.05.085.
[47] C.N. Antonopoulos, G.S. Sfyroeras, J.D. Kakisis, K.G. Moulakakis, C.D. Liapis, The role of soluble P selectin in the diagnosis of venous thromboembolism, Thromb. Res. 133 (1) (2014) 17–24, https://doi.org/10.1016/j.thromres.2013.08.014.
[48] B. Lee, I. Jo, Y. Bu, J. Park, S. Maeng, H. Kang, W. Jang, D. Hwang, W. Lee, K. Min, Antiplatelet effects of Spatholobus suberectus via inhibition of the glycoprotein IIb/IIIa receptor, J. Ethnopharmacol. 134 (2) (2011) 460–467, https://doi.org/10.1016/j.jep.2010.12.039.
[49] W. Han, B. Zhou, K. Yang, X. Xiong, S. Luan, Z. Xu, P. Lei, Z. Luo, J. Gao, Y. Zhan, G. Chen, L. Liang, R. Wang, S. Li, H. Xu, Biofilm-inspired adhesive and antibacterial hydrogel with tough tissue integration performance for sealing hemostasis and wound healing, Bioactive Materials 5 (4) (2020) 768–778, https://doi.org/10.1016/j.bioactmat.2020.05.008.
[50] L.K. Meena, P. Raval, D. Kedaria, R. Vasita, Study of locust bean gum reinforced cyst-chitosan and oxidized dextran based semi-IPN cryogel dressing for hemostatic application, Bioactive Materials 3 (3) (2017) 370–384, https://doi.org/10.1016/j.bioactmat.2017.11.005.
[51] X. Xu, X. Xia, K. Zhang, A. Rai, Z. Li, P. Zhao, K. Wei, L. Zou, B. Yang, W.-Y. C. Philip, Bioadhesive hydrogels demonstrating pH-independent and ultrafast gelation promote gastric ulcer healing in pigs, Sci. Transl. Med. 12 (558) (2020), eaba8014, https://doi.org/10.1126/scitranslmed.aba8014.